INVITED REVIEW

This section of Journal of Materials Research is reserved for papers that are reviews of literature in a given area.

High-entropy functional materials

Michael C. Gao[a),b)]
National Energy Technology Laboratory, Materials Engineering and Manufacturing Directorate, Albany, Oregon 97321, USA; and AECOM, Albany, Oregon 97321, USA

Daniel B. Miracle[b)]
AF Research Laboratory, Materials and Manufacturing Directorate, Wright-Patterson AFB, Ohio 45433, USA

David Maurice
National Energy Technology Laboratory, Materials Engineering and Manufacturing Directorate, Albany, Oregon 97321, USA

Xuehui Yan and Yong Zhang
The State Key Laboratory of Advanced Metals and Materials, University of Science and Technology Beijing, Beijing 10083, People's Republic of China

Jeffrey A. Hawk
National Energy Technology Laboratory, Materials Engineering and Manufacturing Directorate, Albany, Oregon 97321, USA

(Received 27 April 2018; accepted 15 August 2018)

While most papers on high-entropy alloys (HEAs) focus on the microstructure and mechanical properties for structural materials applications, there has been growing interest in developing high-entropy functional materials. The objective of this paper is to provide a brief, timely review on select functional properties of HEAs, including soft magnetic, magnetocaloric, physical, thermoelectric, superconducting, and hydrogen storage. Comparisons of functional properties between HEAs and conventional low- and medium-entropy materials are provided, and examples are illustrated using computational modeling and tuning the composition of existing functional materials through substitutional or interstitial mixing. Extending the concept of high configurational entropy to a wide range of materials such as intermetallics, ceramics, and semiconductors through the isostructural design approach is discussed. Perspectives are offered in designing future high-performance functional materials utilizing the high-entropy concepts and high-throughput predictive computational modeling.

I. INTRODUCTION

Contrasted to traditional alloys that focus on the compositions on the boundaries (vertices, edges, or faces) of phase diagrams, high-entropy alloys (HEAs),[1] or multiprincipal-element alloys (MPEAs),[2] focus on compositions proximal to the center of multicomponent phase diagrams. The vast HEA composition space and resulting varying materials properties represent a scientifically challenging and technologically important research frontier for materials scientists and engineers to explore. Single-phase solid-solution HEAs[3] [e.g., with the face-centered cubic (FCC), body-centered cubic (BCC), and hexagonal close-packed (HCP) structures] may have large configurational entropies, but they also have limited use since many applications require balanced properties. For example, structural materials often require multiple phases to achieve the required balance of properties. Thus multiphase solid solution HEAs are often more appropriate for structural materials applications. For the current understanding and challenges on HEA research, the readers are referred to recent review reports.[4–6]

To date, the vast majority of the research on HEAs has focused on their potential applications as structural materials, and accordingly, by manipulating the compositions, processing, and hence microstructures, balanced mechanical properties are achieved that are consistent with, and sometimes superior to, traditional materials.[4–10] However, there has been increasing interest in HEAs for their functional properties.[11] Many papers are dedicated to the study of the soft magnetic properties of HEAs that comprise magnetic elements Co, Fe, Ni, and Mn, with the addition of other elements, aiming to reach high saturation magnetization and low coercivity. Magnetic HEAs may possess an

[a)]Address all correspondence to this author.
e-mail: Michael.Gao@netl.doe.gov
[b)]These authors were editors of this journal during the review and decision stage. For the *JMR* policy on review and publication of manuscripts authored by editors, please refer to http://www.mrs.org/editor-manuscripts/.
DOI: 10.1557/jmr.2018.323

enhanced magnetocaloric effect (MCE) because the extreme chemical disorder in HEAs is expected to result in sluggish magnetic phase transitions during cooling. This would open the door for HEAs as next-generation magnetic refrigerant materials.[12,13] Significantly reduced thermal conductivity due to extreme chemical disorder in HEAs makes them attractive as potential thermoelectric materials.[14–16] Electrochemical properties,[11,17–19] high-entropy coatings,[20] as well as other novel ideas[21] have also been reported.

In addition, conventional alloying strategies used in the functional materials community—preceding the initial high entropy papers in 2004—have produced a vast literature of functional HEAs and MPEAs, which may be missed by conventional literature searches. Many functional materials have been studied, which satisfy HEA definitions or are consistent with the broader concept of MPEAs,[6] but they have not been identified with the HEA concept. Since conventional efforts to develop functional materials precede the high-entropy concept and since early work in the high-entropy field focused on structural properties, these two communities appear to be rather disconnected. There are two important benefits to connect traditional functional materials research with high-entropy concepts. First, the HEA community benefits by accessing a vast amount of existing data on functional MPEAs that have already been made and characterized. This knowledge can be used to validate existing HEA concepts and to develop new relationships between composition, phase stability, and properties. Second, the functional materials community benefits by accessing new knowledge and tools for designing materials with targeted crystal structures and properties.

This paper provides a timely and brief review on select high-entropy functional materials. Medium- and even low-entropy materials based on known commercial compounds, which have been developed to tailor the cost and required properties, are also covered. Throughout the paper, perspectives are offered in designing future high-performance functional materials.

II. MAGNETIC PROPERTIES

A. Soft magnets

Soft magnetic materials magnetize to saturation when subjected to a relatively weak magnetic field (i.e., high permeability) and demagnetize and reverse polarity when subjected to a relatively weak magnetic field of opposing polarity (i.e., low coercivity). The key magnetic characteristics that define this class is a low intrinsic coercivity ($_iH_c < \sim 1$ kAm^{-1}). This ease of magnetization and demagnetization—or the ability to switch between these states—renders them useful for two broad classes of applications. First, they are useful in conversions between electromagnetic energy and mechanical energy, and as such, have extensive applications in the power grid. They can be found in components used for the generation, transmission, and distribution of electric power, as well as in transformers. Second, these materials can also be used in signal processing equipment, such as controls, telecommunications, computers, transducers, and magnetic recording equipment.

These two broad classes of applications have different performance requirements. In fact, the myriad end uses result in a considerable spectrum of material compositions and properties. One desirable characteristic consistent across these applications is a high value of magnetic saturation (M_s). High magnetic saturation enables the smallest magnet for a given switching energy requirement. In many of these applications, the individual magnets can be quite small, but the number required can be extremely large. A high saturation magnetization is best achieved with a material made using predominantly ferromagnetic elements such as iron.

In addition to high magnetic saturation, a high electrical resistivity is desired as this prevents eddy current losses. For elevated temperature applications, a high Curie temperature (T_C) is required. Resistivity in soft magnetic materials is typically enhanced by alloying with nonmetallic elements. These elements have a greater intrinsic resistivity and they tend to increase lattice distortion, both of which improve overall resistivity. Changing the Curie temperature of a magnetic material can be done by doping, or by changing the sizes of particles in the lattice, thereby modifying the lattice structure (and thus coordination number), and coincidentally by inducing strains.

HEAs are expected to have a reduced saturation magnetization due to the lower concentration of elements with the highest net magnetic moments. The presence of nonmagnetic principal elements reduces the total magnetization per formula unit. The chemical disorder in these simple FCC, BCC, and HCP solid solutions also makes any magnetic reordering more difficult than traditional magnetic compounds, which is expected to raise coercivity.

A comprehensive sampling of reported investigations on magnetic HEAs is given in Refs. 22–50, and the reported magnetic properties are summarized in Table I, categorized according to alloy microstructures from single FCC, single BCC, to FCC + BCC phases, FCC (BCC) + intermetallics (IM), and amorphous structures. All alloys that satisfy the HEA definitions[51] indeed have relatively low M_s values, typically less than 1 T. The medium-entropy alloy CoFeNi has the highest M_s at 1.606 T in Table I, and doping with Al and Si at low levels can result in optimal properties, e.g., in CoFeNi $(AlSi)_{0.2}$: M_s (1.15 T), H_c (1400 A/m), resistivity (69.5 μΩ cm), yield strength (342 MPa), and compression plastic strain (>50%).[29] Among the crystalline alloys studied, the $Co_{20}Cr_{20}Fe_{20}Mn_5Ni_{20}Zn_{15}$ alloy after mechanical alloying and annealing has the highest H_c value of 40,982 A/m, while CoCrFeNi has the lowest H_c value of 46 A/m. By contrast, the amorphous HEAs have $H_c \sim 1$ T and $M_s \sim 2$ A/m.

TABLE I. Measured saturation magnetization (M_s, T) versus coercivity (H_c, A/m) for HEAs reported in the literature.

Alloy	Structure	H_c (A/m)	M_s (T)	Condition	Ref.
CoFeNi	FCC	120.93	1.606	...	33
CoFeNi	FCC	1069.08	1.356	...	29
CoFeNi	FCC	189.0	1.671	...	45
CoCrFeNi	FCC	46.15	0.200	T = 50 K	25
CoCrFeNi	FCC	1251.75	0.144	MA + VHPS	47
CoFeMnNi	FCC	119.00	0.188	...	46
$Al_{0.25}$CoCrFeNi	FCC	355.71	0.151	T = 50 K	25
$Al_{0.25}$CoFeNi	FCC	215.61	1.287	...	33
$Al_{0.25}CoFeMn_{0.25}Ni$	FCC	268.0	0.999	~800	41
CoCrFeMnNi	FCC		Paramagnetic down to 93 K		49
CoCrFeMnNi	FCC	13980.17	0.951	MA	35
CoCrFeMnNi	FCC	~0	0.328	SPS	35
CoCrFeMnNi	FCC	10804.0	0.014	...	46
CoCrFeNiTi	FCC	11900.01	0.220	As-synthesized	44
CoCrFeNiTi	FCC	9660.70	0.013	Annealed	44
CoCrCuFeNi	FCC	13209.86	0.559	MA-HPS	38
$CoFeNiSi_{0.25}$	FCC	352.45	1.216	...	33
$CoFeNi(AlSi)_{0.1}$	FCC	1088.93	1.287	...	29
$CoFeNi(AlSi)_{0.2}$	FCC	1400.72	1.130	...	29
CoCrFeMnNi	FCC	...	0.014	MA-HPS	38
CoCrFeNiPd	FCC	...	0.378	...	26
$CoCrFeNiPd_2$	FCC	...	0.413	...	26
CoCrCuFeNi	FCC	...	0.044	MA + VHPS	47
CoCrCuFeNi	FCC	...	0.016	Paramagnetic	22
$CoCrCuFeNiTi_{0.5}$	FCC	...	0.003	Paramagnetic	22
$CoFeNi(AlCu)_{0.2}$	FCC	...	1.361	...	48
$CoFeNi(AlCu)_{0.4}$	FCC	...	1.065	...	48
$FeCoNi(AlCu)_{0.6}$	FCC	...	0.848	...	48
AlCoCrFeNi	BCC	4138.03	0.546	...	28
$Al_{1.25}$CoCrFeNi	BCC	2911.74	0.656	T = 50 K	25
Al_2CoCrFeNi	BCC	187.80	0.267	T = 50 K	25
$AlCoCrFeNb_{0.1}Ni$	BCC	4615.49	0.422	...	28
Al_2CoCrFeNi	BCC	...	0.096–0.133	...	26
$Al_{0.5}$CoCrFeNi	FCC + BCC	755.99	0.143	T = 50 K	25
$Al_{0.75}$CoCrFeNi	FCC + BCC	362.87	0.087	T = 50 K	25
$CoFeNi(AlCu)_{0.8}$	FCC + BCC	362.0	0.714	...	50
$CoFeNi(AlMn)_{0.5}$	FCC + BCC	730.0	0.482	...	45
$CoFeNi(AlMn)_{0.75}$	FCC + BCC	445.0	1.148	...	45
$CoFeNi(AlCu)_{0.8}Ga_{0.02}$	FCC + BCC	380.50	0.717	...	50
$CoFeNi(AlCu)_{0.8}Ga_{0.04}$	FCC + BCC	383.40	0.722	...	50
$CoFeNi(AlCu)_{0.8}Ga_{0.06}$	FCC + BCC	464.10	0.733	...	50
$CoFeNi(AlCu)_{0.8}Ga_{0.08}$	FCC + BCC	685.80	0.749	...	50
$Al_{0.5}$CoFeNi	FCC + BCC	342.90	0.992	...	33
$Al_{0.75}$CoFeNi	FCC + BCC	307.90	0.985	...	33
AlCoFeNi	FCC + BCC	224.36	0.846	...	33
$CoFeNi(AlSi)_{0.3}$	FCC + BCC	19335.71	0.900	...	29
$CoFeNi(AlSi)_{0.4}$	FCC + BCC	17963.37	0.904	...	29
$CoFeNi(AlSi)_{0.5}$	FCC + BCC	1937.0	0.865	...	29
$CoFeNi(AlSi)_{0.8}$	FCC + BCC	5951.51	0.423	...	29
AlCoCrCuFeNi	FCC + BCC	3580.99	0.339	As-cast	24
AlCoCrCuFeNi	FCC + BCC	1193.66	0.143	Annealed	24
CoFeGaMnNi	FCC + BCC	915.0	0.763	...	46
$CoFeNi(AlCu)_{0.7}$	FCC + BCC	...	0.762	...	48
$CoFeNi(AlCu)_{0.8}$	FCC + BCC	...	0.723	...	48
$CoFeNi(AlCu)_{0.9}$	FCC + BCC	...	0.805	...	48
$CoFeNi(AlCu)_{1.0}$	FCC + BCC	...	0.750	...	48
$CoFeNi(AlCu)_{1.2}$	FCC + BCC	...	0.643	...	48
$CoFeNiSi_{0.5}$	FCC + Ni_3Si	408.23	0.816	...	33
$CoFeNiSi_{0.75}$	FCC + Ni_3Si	4531.93	0.671	...	33
CrFeNiTi	FCC1 + FCC2 + σ	13283.87	0.118	As-synthesized	44

(continued)

TABLE I. Measured saturation magnetization (M_s, T) versus coercivity (H_c, A/m) for HEAs reported in the literature. (continued)

CrFeNiTi	FCC1 + FCC2 + σ	12161.03	0.008	Annealed	44
CrFeMnNiTi	FCC1 + FCC2 + σ	17970.98	0.020	As-synthesized	44
CrFeMnNiTi	FCC1 + FCC2 + σ	10430.22	0.004	Annealed	44
CoFeMnNiSn	$L2_1$ + BCC	3431.0	0.797	...	46
AlCoFeMnNi	BCC + B2	629.0	1.260	...	46
$Fe_{40}Co_{35}Ni_5Al_5Cr_5Si_{10}$	BCC + B2	79.60	1.145	Thin film, annealed	39
$AlCoCrFeNb_{0.25}Ni$	BCC1 + BCC2 + Laves	7480.28	0.298	...	28
$AlCoCrFeNb_{0.5}Ni$	BCC1 + BCC2 + Laves	6764.09	0.154	...	28
$AlCoCrFeNb_{0.75}Ni$	BCC1 + BCC2 + Laves	7480.28	0.091	...	28
$Co_{20}Cr_{20}Fe_{20}Mn_5Ni_{20}Zn_{15}$	FCC + multiphases	40982.40	0.499	...	40
$Co_{26.7}Fe_{26.7}Ni_{26.6}Si_9B_{11}$	Amorphous	2.0	1.070	...	42
$B_{15}Co_{25}Fe_{25}Ni_{25}Si_{10}$	Amorphous	2.30	0.840	...	36
$B_{17.5}Co_{25}Fe_{25}Ni_{25}Si_{7.5}$	Amorphous	1.10	0.870	...	36
$B_{8.7}Co_{28.5}Fe_{26.7}Ni_{28.5}P_3Si_{4.6}$	Amorphous	4.00	1.070	...	43

MA = mechanical alloying, VHPS = vacuum hot-pressing sintering, HPS = high pressure sintering, SPS = spark plasma sintering.

In examining the literature, a wide range in magnetic properties (Table I) may exist for any given alloy. This results from variations in real sample chemistry and density, the consolidated states of the sample (i.e., as-cast versus homogenized or annealed versus mechanically alloyed, bulk versus thin film, etc.), and the magnetic testing parameters. As an extreme example of how sample state may affect measurements, Schneeweiss[49] reported that the FCC CoCrFeMnNi alloy is paramagnetic down to 93 K, at which point it transits into the (super)spin glass state, while a second magnetic transformation of a ferromagnetic type occurs at 38 K.

The observed data scattering indicates the very real necessity of standardizing testing procedures and reporting on materials variables (and their complete pedigree) which can influence properties. The ideal sample for magnetic testing is spherical and roughly 2–3 mm in diameter; if other geometries are used, then proper field corrections must be applied and reported. Sample density also has a strong effect on measurements, and coercivity is affected by microstructural defects such as dislocations, grain boundaries, and phase interfaces. Evaluating and reporting on the starting state and these other characteristics would enable better identification and further development of interesting alloys.

In Fig. 1, the measured magnetic properties of select HEAs (Table I) are overlaid on a map of saturation magnetization versus coercivity for major conventional soft and semihard magnetic materials.[52] The comparison shows that the projected trends of lower saturation magnetization and higher coercivity of HEAs compared to traditional soft magnets hold true in practice.

Superior soft magnets require low magnetocrystalline anisotropy and low magnetostriction.[53] Alloying elements, phase structure, and microstructure have a great impact on both parameters and hence soft magnetic properties. To increase M_s, the basic design principle is to increase the contents of ferromagnetic elements, while reducing nonferromagnetic (and especially the antiferromagnetic) elements. This will refine the compositional space of interest. The coercivity of magnetic materials mainly depends on the resistance of magnetic domain rotation and magnetic domain wall movement, with greater resistance resulting in higher coercivity. The introduction of nonferromagnetic elements can result in partial pinning of domain walls.

While not considerations for magnetic performance, due to the environments in which soft magnets are used, corrosion resistance and wear resistance can be factors in the selection of which magnetic alloy to use. Based upon these well-established phenomena and those of HEAs, it is possible to hypothesize how soft magnetic HEAs may differ from the well-established soft magnetic alloys. This is shown in Table II. Soft magnetic HEAs feature excellent mechanical properties and are expected to offer superior corrosion resistance.

While this subsection has described general preferences in magnetic properties, soft magnet manufacturers often produce an extensive selection of magnets. Within this selection, any magnet represents some set of compromises, including cost considerations, and many are tailored to specific applications. Selection of a soft magnetic material is often a nontrivial exercise. Accordingly, the projected trends in Table II should not be viewed as "better" or "worse," but rather as starting points for evaluating potential applications.

B. Theoretical calculations

With vast compositional spaces available for experimenting, the computational design of alloys offers the advantage of reducing the resource demands of early-stage alloy development. This section takes a look at the degree to which the magnetic properties of potential alloys agree with theoretical predictions.

Intrinsic magnetization can be predicted using first-principles density functional theory (DFT) calculations. Zuo et al.[46] calculated the electronic structures and

magnetic properties of FCC CoFeMnNi, FCC CoFeMnNiCr, and BCC CoFeMnNiAl at zero Kelvin. The calculated average magnetic moments were 0.89, 0.39, and 1.23 μ_B/atom (μ_B = Bohr magneton), respectively. The Curie temperature was determined to be ~120–130 K for CoFeMnNi.[25,54] It was measured to be ~38 K[49] and predicted to be ~20–27 K[55,56] for FCC CoCrFeMnNi. Figure 2 compares the distribution of magnetic moment per element in these alloys predicted from DFT. The addition of Cr to CoFeMnNi lowers the magnitude of the magnetic moment and causes larger scattering in the moment of the atoms, suggesting sensitivity of the moment to neighboring atoms due to the Cr addition. On the other hand, the addition of Al to CoFeMnNi reduces the number of down-spins for Mn, and thus, causes the alloy to behave ferromagnetically. The total electron density of states (DOS) calculations show that the up and down spins of CoFeMnNi and CoFeMnNiCr are more symmetric than CoFeMnNiAl, while there is a significantly higher spin-up distribution than the spin-down distribution in CoFeMnNiAl.[46]

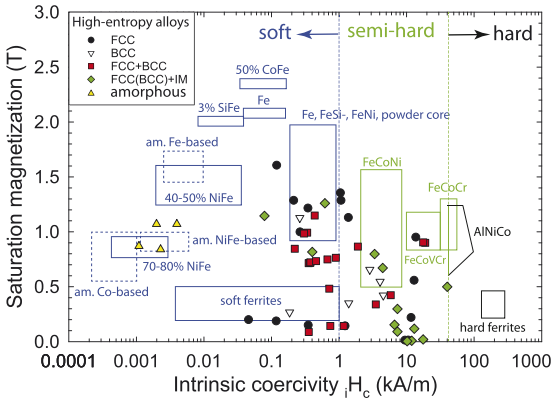

FIG. 1. Measured saturation magnetization versus coercivity of HEAs with the structures of FCC, BCC, FCC + BCC, FCC (BCC) + intermetallics (IM), and amorphous (Table I) compared with major conventional soft and semihard magnetic materials (adapted with permission from Ref. 52).

The magnetic exchange in magnetic alloys can be examined by the parameter: $J'_{ij} = z_p J_{ij} m_i m_j$, where $m_i(m_j)$ is the magnetic moment of element $i(j)$, J_{ij} is the strength of the exchange interaction between elements i and j, and z_p is the coordination number of the pth coordination shell. Huang et al.[56] studied the exchange interaction of CoCrFeMnNi in FCC and BCC structures and predicted a weaker magnetic ordering tendency and a lower critical temperature for the FCC structure than the BCC structure. The magnetic behavior of the BCC phase is dictated by strong nearest-neighbor Fe–Fe, Fe–Co, Co–Co, and Co–Mn pairs, and the antiferromagnetic interactions between the nearest-neighbor Cr–Cr, Cr–Mn, and Mn–Mn pairs. Whereas for the FCC structure, the magnetic behavior is mainly due to the nearest-neighbor antiferromagnetic couplings between Fe–Mn and Mn–Mn.

Other magnetic properties of metals and alloys, such as the Curie temperature, can be predicted using DFT calculations by coupling the Heisenberg model and Monte Carlo simulations.[57,58] An alternative but much simpler approach for calculating the Curie temperature is to use the mean-field approximation:

$$k_B Tc = 2(E_{FM} - E_{PM})/3(1-c) \quad , \qquad (1)$$

where k_B is the Boltzmann constant, c is the mole fraction of the nonmagnetic element, and E_{FM} and E_{PM} are the total energies of the alloy in the ferromagnetic and paramagnetic states, respectively. Using this approach, Körmann et al.[58] obtained good agreement for Curie temperature between calculations and experiments in $CoFeNiCr_{0.5}$, CoFeNiCr, CoFeNiCrPd, $CoFeNiCrPd_2$, $CoFeNiCr_{0.5}Pd_x$, $CoFeNiCrPd_x$, $CoFeNiCr_xPd_2$, $CoFeNiCr_xPd$, and $CoFeNiCr_x$. Körmann et al.[58] further mapped the Curie temperature and saturation magnetization of $CoCrFeNi–Cr_x–(Ag,Au,Cu,Pd)_y$ alloys at zero temperature.

Using the mean-field approach, Huang et al.[56] mapped out the Curie temperatures of many medium- and high-entropy alloys with the FCC and BCC structures (see Fig. 3). The calculated T_C values are lower for the

TABLE II. Projected trends in the performance of HEA magnets.

Property	Projected trend (HEA versus conventional)	Rationale for projection
Saturation magnetization (M_s)	Lower	Lower content of ferromagnetic elements
Intrinsic coercivity ($_iH_c$)	Higher	Lattice structures will tend to pin domain walls
Permeability (μ)	Lower	Lower content of high permeability elements
Electrical resistivity	Higher	Greater lattice distortion; potentially higher content of nonmetallic elements
Curie temperature (T_C)	May be higher or lower	Less compact lattices tend to reduce T_C; smaller particle sizes tend to reduce T_C; changes in crystal structure and in alloying elements can raise or lower T_C
Corrosion resistance	Higher	Cocktail effect promotes the formation of various surface oxide films
Wear resistance	Higher	Severe lattice distortion tends to improve hardness and strength, and high temperature softening resistance tends to facilitate high wear resistance

FCC structure than for the BCC. Agreement with experiments for those FCC HEAs, where available, is satisfactory overall, except for CrFeCoNiCu, FeCoNiCuMo, and MnFeCoNiCu that do not form single-phase FCC solid solution in the as-cast form. It is worth noting that some alloys with high fractions of magnetic elements are predicted to have relatively higher Curie temperatures: CoFeNi (804 K), CoCuFeNiPt (837 K), AgCoCuFeNi (805 K), and CoCuFeNi (796 K). However, with increasing fractions of nonmagnetic elements, the calculated Curie temperature drops to as low as 10 K for CoCrFeMnNiV, 21 K for CrFeMoV, and 27 K for MnCoFeMnNiV. In general, it is anticipated that HEAs will typically have significantly lower T_C than traditional low-entropy magnetic alloys.

These theoretical studies[37,46,56,58] suggest that DFT calculations can be useful in predicting magnetic properties such as magnetization and critical magnetic ordering temperatures and thus can be used to accelerate the development of high-entropy magnetic alloys.

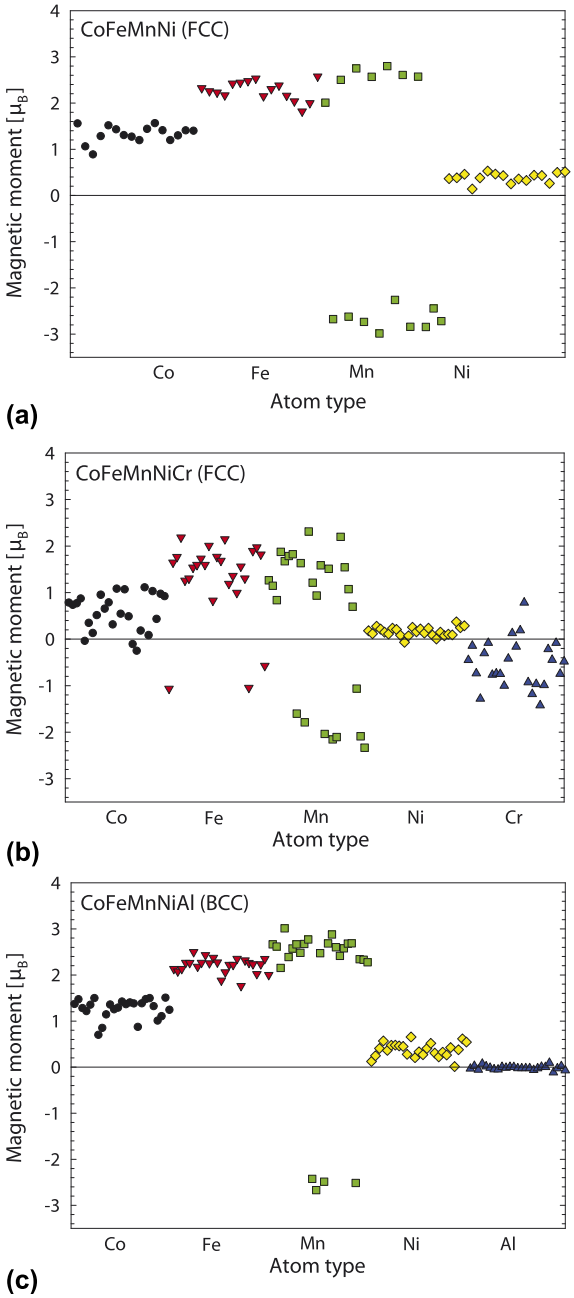

FIG. 2. Magnetic moments of individual atoms at zero temperature[46] in (a) FCC CoFeMnNi, (b) FCC CoFeMnNiCr, and (c) BCC CoFeMnNiAl predicted from DFT calculations (reprinted with permission from Ref. 46).

C. MCE

The MCE refers to the temperature change that a magnetic material experiences when an external magnetic field is applied and withdrawn adiabatically.[12] When a magnetic field is applied, the magnetic domains of a material tend to align with the applied field, thereby decreasing the magnetic entropy (ΔS_M). Accordingly, the thermal entropy of the system increases while the total entropy change remains zero, increasing the temperature of the system. The opposite occurs when the field is removed. The magnetic entropy change is defined as

$$\Delta S_M = \int_0^H \left(\frac{\partial M}{\partial T}\right)_H \mathrm{d}H \quad . \tag{2}$$

The refrigerant capacity (RC) value has been commonly used for comparing magnetocaloric materials, which considers the temperature range and the magnetic entropy. RC is generally determined as the product of the magnetic entropy and the temperature span at the full width, half maximum of the entropy curve:

$$\mathrm{RC} = \left|\Delta S_M \Delta T_{\mathrm{FWHM}}\right| \quad . \tag{3}$$

Both the peak value of ΔS_M and the integrated area under the ΔS_M–T curve are used to calculate RC.[13]

Chemical disorder in HEAs may cause sluggish magnetic phase transitions during cooling, resulting in an enhanced MCE. Therefore, magnetic HEAs are potentially attractive candidates for magnetic refrigerants due to their improved MCEs. A collection of MCE HEAs is summarized in Table III, and comparison in their RC and ΔS_M is shown in Fig. 4. For example, Yuan et al.[13] studied the microstructure and magnetic properties of DyErGdHoTb, ErGdHoTb, DyErHoTb, and ErHoTb alloys and found that the quinary DyErGdHoTb alloy with the HCP structure exhibited a small magnetic hysteresis and possessed the largest RC among the alloys they studied (about 627 J/kg at the 5 T magnetic field). Their work also demonstrates that including Gd is critical which increases the critical magnetic ordering temperature and enhances the RC value.

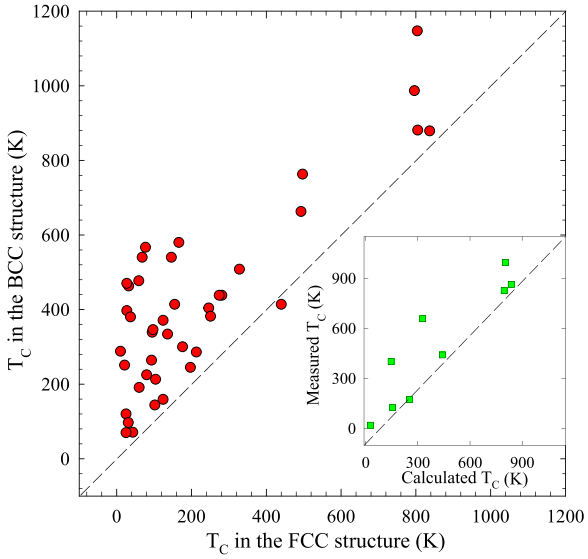

FIG. 3. Calculated Curie temperatures (T_C) for 42 multicomponent equimolar alloys with the FCC and BCC structures (filled circles in red). The inset compares the calculated T_C values with experiments for select single-phase FCC alloys (filled squares in green) (adapted with permission from Ref. 56).

By contrast, the $|\Delta S_M|$ and RC values for Co–Cu–Fe–Mn–Ni[12] and $CoCrFeNiPd_x$[59] HEAs are too low for commercial refrigeration application (Fig. 4 and Table III); however, these HEAs have advantages in cooling power, ductility, machinability, resistance to wear and corrosion, reduced metal flammability, and structural integrity,[59] making them promising for use in extreme environments and active cooling.[12,59] For comparison with traditional magnetocaloric materials, readers are referred to original publications.[12,13,59]

In a recent review article on conventional magnetocaloric materials, Shen et al.[60] highlighted $La(Fe,M)_{13}$-based compounds (M = Si, Al) for their remarkable MCE in comparison with other magnetocaloric materials including NiMn-based Heusler alloys, $Ce_6Ni_2Si_3$-type $R_6Co_{1.67}Si_3$ compounds, AB_2X_4-type sulfospinels $CdCr_2S_4$, etc. They found a large entropy change [$|\Delta S_m| > 19$ J/(kg K) with $T_C < 210$ K] for a field change of 0–5 T in $La(Fe,Si)_{13}$ with a low Si concentration, and this change was associated with negative lattice expansion and metamagnetic transition behavior.

Doping using the iso-structure method is commonly used in conventional magnetocaloric materials research. For example, by mixing rare-earth elements in $(La_{1-x}Pr_x)Fe_{11.5}Si_{1.5}$ alloys, Shen et al.[61] found that $|\Delta S_m|$ increased with increasing Pr molar ratio, achieving the maximum $|\Delta S_m|$ at equimolar ratios of La and Pr (see Fig. 5). By contrast, a significant decrease in $|\Delta S_m|$ was observed when Fe was substituted for Co in $(La_{1-x}Pr_x)(Fe_{11.5-y}Co_y)Si_{1.5}$,[61] although Co doping results in significantly larger configurational entropies than Pr doping.

TABLE III. Applied magnetic field, magnetic entropy changes (ΔS_M), and refrigerant capacity (RC) for reported HEAs.

Composition	Applied field (T)	$\lvert\Delta S_M\rvert$ (J/kg/K)	RC (J/kg)	Ref.
CoCuFeMnNi	1.5	0.115	16.5	12
$CoCu_{0.975}FeMn_{1.025}Ni$	1.5	0.094	15.3	12
$CoCu_{0.95}FeMn_{1.05}Ni$	1.5	0.10	13.5	12
$CoCu_{0.925}FeMn_{1.075}Ni$	1.5	0.084	12.2	12
$CoCu_{0.9}FeMn_{1.1}Ni$	1.5	0.081	9.6	12
$CoCuFe_{0.975}Mn_{1.025}Ni$	1.5	0.105	14	12
$CoCuFe_{0.95}Mn_{1.05}Ni$	1.5	0.071	10	12
$CoCrFeNiPd_x$	5	<0.9	<175	59
DyErGdHoTb	5	8.6	627	13
ErGdHoTb	3	4.8	137	13
DyErHoTb	3	0.65	27.3	13
ErHoTb	3	3	150	13

The contrasting behavior in $|\Delta S_m|$ versus ΔS_{conf} suggests other mechanisms contribute much more to the magnetic entropy change than configurational entropy does. Partial substitution for La leads to a reduction in T_C and an increase in magnetic hysteresis. Conversely, Co doping results in a significant increase in T_C and zero hysteresis loss near room temperature. An additional doping strategy explored was to introduce interstitial atoms such as hydrogen. For example, a maximal value of $|\Delta S_m| = 20.5$ J/(kg K) at 340 K was observed for a field change of 0–5 T for $LaFe_{11.5}Si_{1.5}H_\delta$, which exceeds that of Gd by a factor of 2. Introducing interstitial carbon atoms can thus depress hysteresis loss while keeping the large MCE unchanged.[60]

III. PHYSICAL PROPERTIES

Jin and Bei[62] surveyed and compared the electrical resistivity and thermal conductivity of a series of Ni-containing composition-concentrated FCC solid solution alloys with commercial alloys and bulk metallic glasses (BMG) (see Fig. 6). The overall trend for FCC Ni-alloys is that increasing entropy results in increased electrical resistivity, but not always [Fig. 6(a)]. A noteworthy exception is that Cr-containing HEAs have significantly higher resistivity than those without Cr by about one order of magnitude, regardless of the configurational entropies of these alloys. Electronic structure calculations reveal[63] that alloying with Cr promotes d-band smearing in both minority and majority spin channels, resulting in a much reduced electron mean free path and hence high electrical resistivity.[63] Conversely, for those Ni alloys that do not contain Cr, the majority spin channel has a large (or infinite) electron mean free path, providing a short circuit and hence an overall low resistivity.[63] The electrical resistivities of CoCrNi, CoCrFeNi, $Al_xCoCrFeMn$, CoCrFeMnNi, and CoCrFeNiPd are slightly higher than those of 304 and 316 stainless steels,

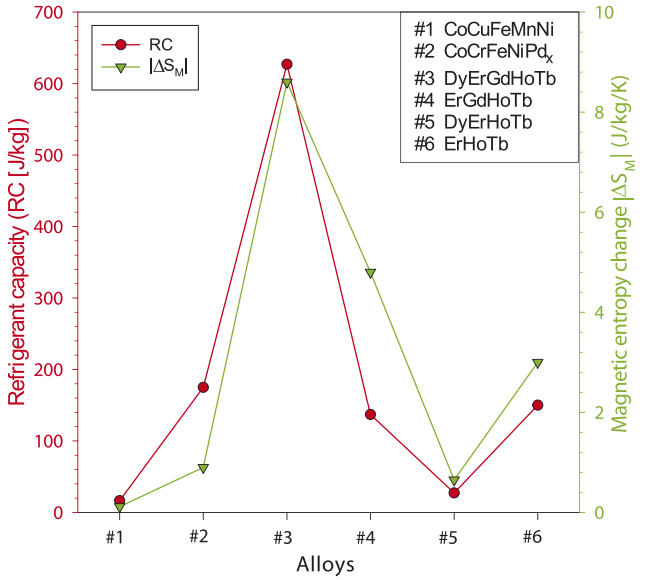

FIG. 4. RC (filled circles in red) and magnetic entropy change $|\Delta S_M|$ (filled triangles in green) of select medium- and high-entropy alloys (data taken from Refs. 12, 13, and 59).

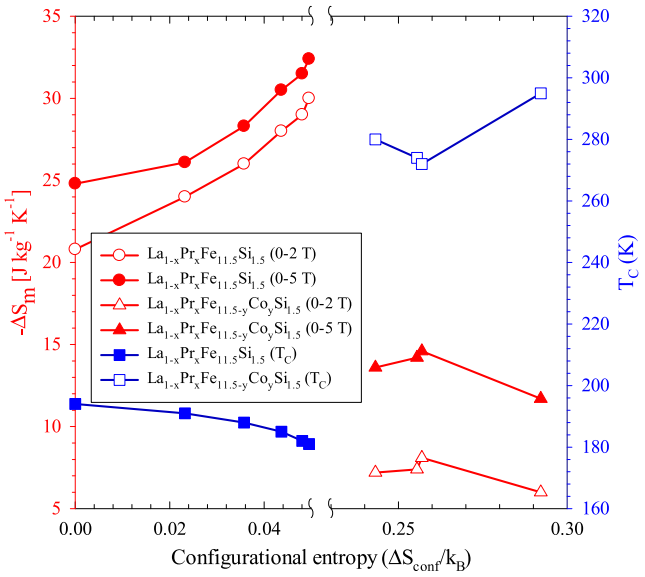

FIG. 5. Magnetic entropy changes ($|\Delta S_M|$) (circles and triangles in red) and Curie temperature (T_C) (squares in blue) as a function of configurational entropy from the substitution in the La and Fe sites in $La_{1-x}Pr_xFe_{11.5}Si_{1.5}$ and $La_{1-x}Pr_xFe_{11.5-y}Co_ySi_{1.5}$ (data taken from Ref. 61).

are comparable to those of Inconel 625 and 718, and are smaller than those of the Ni-containing BMG.

Similar to the case of electrical resistivity, alloying reduces the thermal conductivity of Ni, but thermal conductivity is sensitive to both configurational entropy and alloying elements [Fig. 6(b)]. For Cr-containing FCC alloys with 2–5 components, the thermal conductivities are ~10–15 W/(m K) at room temperature regardless of the compositions and number of principal components. These values are significantly lower than those alloys without Cr, comparable to the values for stainless steels and Inconel alloys, but higher than BMGs [~4–8 W/(m K)]. Thermal conductivity is comprised of electronic and lattice contributions. Contrasted to pure metals for which the electronic contribution is dominant, HEAs have a significantly enhanced lattice contribution compared to electronic contribution [Fig. 6(c)]. Note that the low-entropy Ni–20Cr binary alloy has values of electrical resistivity, thermal conductivity, and lattice contribution to thermal conductivity, all of which are comparable to HEAs (i.e., with 4 or more principal components).

IV. THERMOELECTRIC PROPERTIES

Thermoelectric materials convert between thermal energy and electrical energy: A temperature difference creates an electric potential; an electric potential creates a temperature difference. The ability of a given material to efficiently produce thermoelectric power is measured by its dimensionless figure of merit (zT), given by

$$zT = \frac{\sigma S^2 T}{\kappa} \quad , \tag{4}$$

where S is the Seebeck coefficient, κ is the thermal conductivity, σ is the electrical conductivity, and T is the temperature. The product σS^2 is also called the "power factor" (PF).

For metals or degenerate semiconductors, the Seebeck coefficient can be determined by[64]

$$S = \frac{8\pi^2 k_B^2}{3eh^2} m^* T \left(\frac{\pi}{3n}\right)^{2/3} \quad , \tag{5}$$

where n is the carrier concentration, k_B is the Boltzmann constant, e is the electron charge, h is the Planck constant, T is temperature, and m^* is the effective mass of the carrier. The electrical conductivity (σ) is determined as $\sigma = ne\mu$, where μ is the carrier mobility.

Ideal thermoelectric materials should possess a high Seebeck coefficient, high electrical conductivity, and low thermal conductivity. However, it is extremely difficult to satisfy these three parameters simultaneously since they are intrinsically intercorrelated. For example, a low carrier concentration leads to a large Seebeck coefficient but also results in low electrical conductivity. Furthermore, material characteristics which result in low thermal conductivity usually result in low electrical conductivity.

As shown in Sec. III, the extreme chemical disorder unique to HEAs can substantially reduce the electron mean free path and hence decrease electrical and thermal conductivity by orders of magnitude, as reported in single-phase FCC HEAs by Zhang et al.[65] and multiphase $Al_xCoCrFeNi$ HEAs by Chou et al.[66] The highly

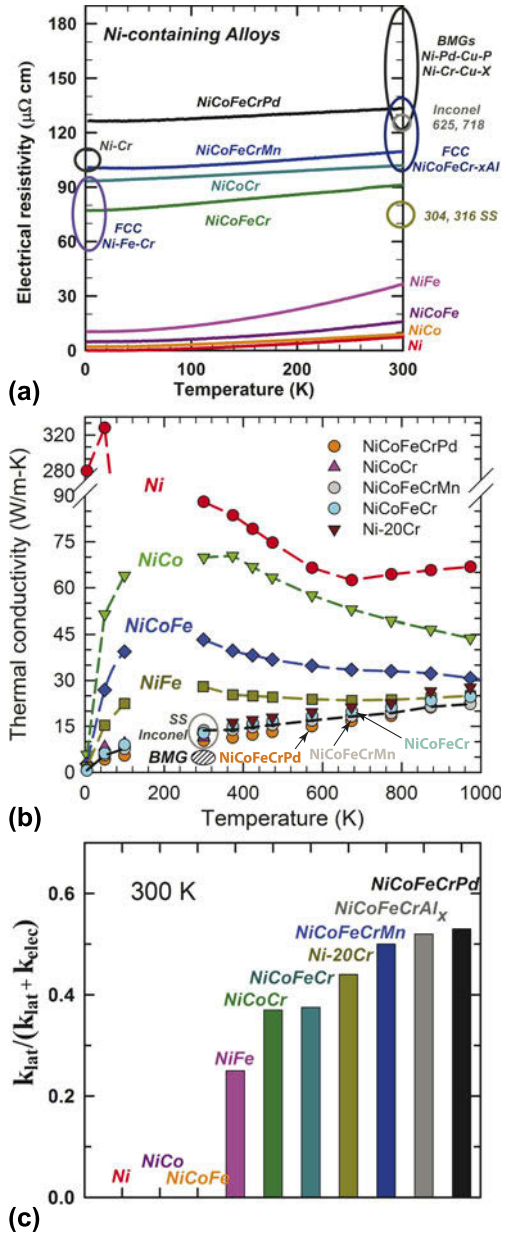

FIG. 6. Comparison in physical properties of Ni-containing FCC HEAs, commercial alloys and BMG: (a) Electrical resistivity, (b) thermal conductivity, and (c) fraction of lattice contribution to thermal conductivity at 300 K. κ_{lat} and κ_{elec} are the lattice and electronic thermal conductivities, respectively (adapted from Ref. 62 Creative Commons License CC BY 4.0—https://creativecommons.org/licenses/by/4.0/).

symmetrical crystal structures (e.g., simple FCC, BCC, and HCP) of HEAs are likely to achieve a high convergence of the valence bands close to the Fermi level to obtain a higher Seebeck coefficient.[67] Therefore, HEAs are promising as thermoelectric materials, especially at high temperatures.

To explore the potential of HEAs as high-temperature thermoelectric materials, Shafeie et al.[14] measured electrical and thermal transport in $Al_xCoCrFeNi$ ($0.00 \le x \le 3.05$) HEAs. With increasing Al contents in $Al_xCoCrFeNi$ HEAs, the Seebeck coefficient increases from 1 to 23 μV/K, thermal conductivity decreases from 15 to 12–13 m/K, and lattice contribution to the thermal conductivity increases, while the electrical conductivity decreases from 0.85 to 0.36 MS m^{-1}. The σS^2 and zT values of $Al_xCoCrFeNi$ HEAs as a function of temperature are shown in Figs. 7(a) and 7(b). The zT is about zero for FCC CoCrFeNi. The highest zT (~0.015) is achieved for $x = 2.0$ and 2.25 at 778 K. Apparently, the $Al_xCoCrFeNi$ HEAs suffer from low Seebeck coefficients and low electrical conductivity.

An ultralow lattice thermal conductivity (i.e., ~0.47 W/(m K) at 400 K) was reported for $BiSbTe_{1.5}Se_{1.5}$ by Fan et al.[16] An increase in the Seebeck coefficient and further decrease in the lattice thermal conductivity can be achieved by doping with Ag [i.e., $(BiSbSe_{1.5}Te_{1.5})_{1-x}Ag_x$ ($0 \le x \le 1.2$)]. A peak zT value of 0.63 was observed at 450 K with the addition of 0.9 at.% Ag. Fan et al.[15] also investigated the thermoelectric performance of PbSeSnTeLa$_x$ ($0 \le x \le 2.5$) HEAs with the FCC structure. HEA PbSeSnTe possesses an ultralow lattice thermal conductivity at low temperatures. Minor additions of La suppressed bipolar transport to some degree, resulting in an enhanced Seebeck coefficient and electrical conductivity at high temperatures. The σS^2 and zT values of $(BiSbTe_{1.5}Se_{1.5})_{1-x}Ag_x$ and PbSeSnTeLa$_x$ HEAs are shown in Figs. 7(c) and 7(d).

The key challenge in developing high-performance thermoelectric HEAs is balancing the electrical conductivity, Seebeck coefficient, and thermal conductivity to maximize zT values. Due to physical intercorrelations among these parameters, predictive computational modeling to calculate thermoelectric properties as a function of temperature plays a crucial role. In addition, methods such as reduced dimension[68,69] and band engineering[70] can be applied to thermoelectric HEAs for enhanced performance.

To develop new materials superior to existing low-entropy thermoelectric materials, doping known thermoelectric materials to promote solid solutions has become a viable approach,[71,72] which also increases the configurational entropy. For example, Tan et al.[71] doped SnTe with >9 at.% Mn, resulting in a high zT equal to 1.3 at 900 K. Manganese doping causes modification of the electronic structure and hence band convergence, resulting in a dramatic increase in the Seebeck coefficient and a decrease in thermal conductivity albeit at the cost of reduced electrical conductivity. A similar approach has been reported by Orabi et al.[72] with Ga doping of SnTe, leading to an 80% improvement in the zT value. Liu et al.[73] assessed the thermoelectric performance of Cu_2(SSeTe)-, (AgCu)(InGa)Te_2-, and $Cu_8Ge(SeTe)_6$-based multicomponent thermoelectric materials. Increasing configurational entropy by doping led to increasing zT values

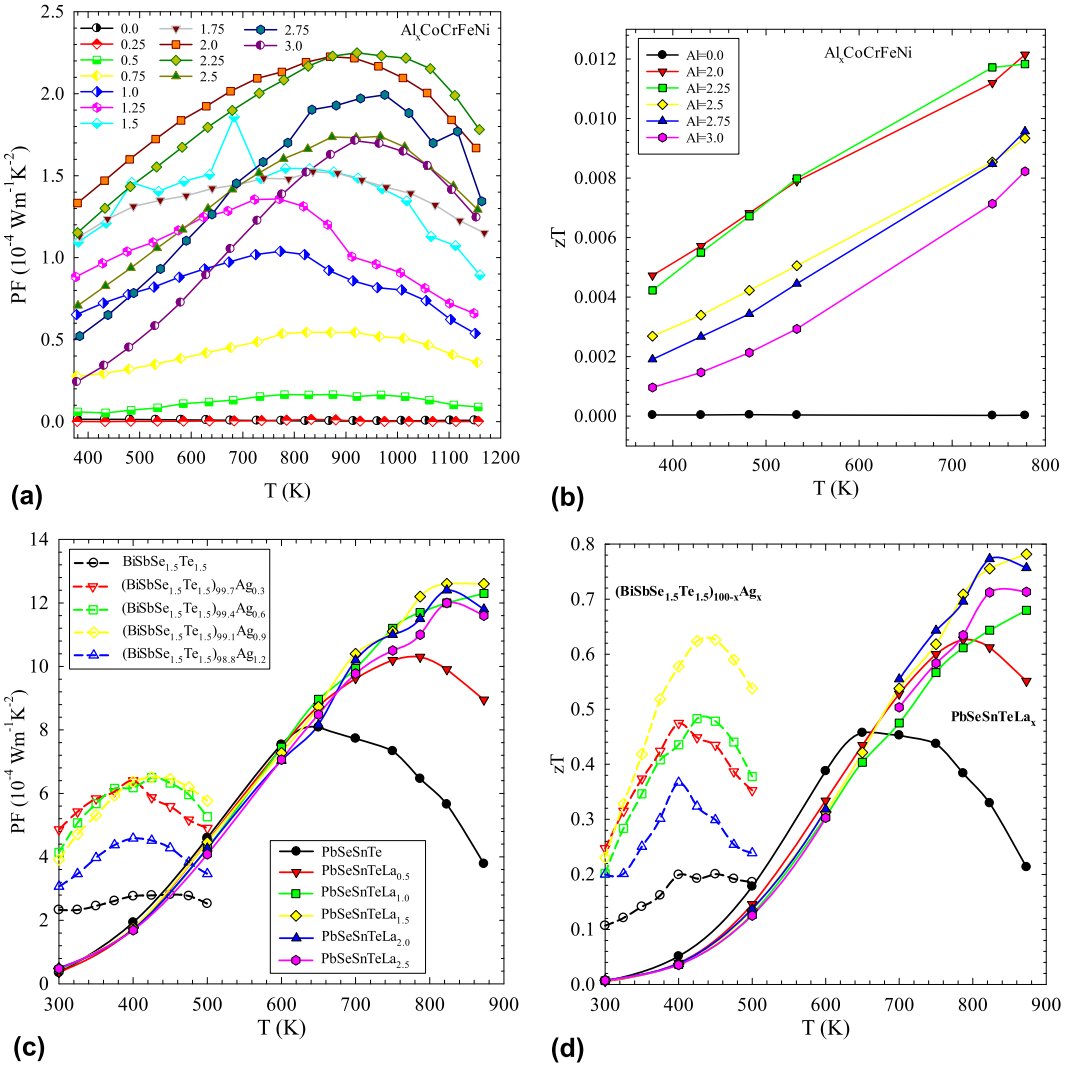

FIG. 7. Determined PFs (a and c) and thermoelectric figure-of-merit (b and d) for $Al_xCoFeMnNi$ HEAs by Shafeie et al.,[14] $PbSeSnTeLa_x$ HEAs by Fan et al.,[15] and $(BiSbSe_{1.5}Te_{1.5})_{1-x}Ag_x$ HEAs by Fan et al.[16] The legends signify the different Al, Ag, and La contents. Parts (a) and (b) have been adapted with permission from Ref. 14. Part (c) is adapted from Ref. 15. Creative Commons License CC BY 4.0—(http://creativecommons.org/licenses/by/4.0/). Part (d) is adapted with permission from Ref. 16.

[Fig. 8(a)], in particular due to significantly reduced thermal conductivity [Fig. 8(b)]. Their survey indicates increasing the entropy by promoting favorable substitution in existing thermoelectric materials can be a viable and cost-effective approach.

V. SUPERCONDUCTING MATERIALS

Superconducting materials (SMs) are functional materials with zero electrical resistance below a critical transition temperature (T_t). As noted by Hott et al.,[74] superconductivity is a true thermodynamic state of matter. The explanation for this state and the conditions, which are requisite for achieving this state, are less well established. In a recent review by Chu et al.,[75] multiple prominent researchers in the field offered ideas on how to find future SMs. Difficulty in establishing criteria for finding new SMs was often cited as the main impediment to future alloy discovery. For example, one group examined over 1000 materials considered to be likely candidates, but only had a 3% success rate.[75] There may be some commonalities to this group's suggested criteria which make for appropriate starting points for exploring HEA space for superconductors, including (i) magnetism, (ii) layered crystal structures, (iii) the incorporation of transition metals, and (iv) valence electron/carrier densities within a certain range.

There have been HEA superconductors discovered to date, which seem to offer some interesting properties. For example, Kozelj et al.[76] reported the superconductivity of HfNbTaTiZr system alloys. They found that the electronic properties were not a "cocktail" of the constituent

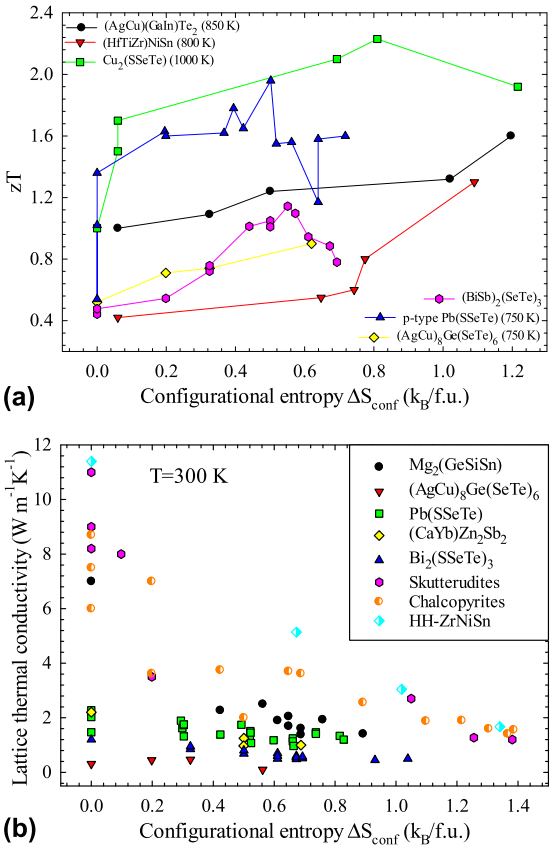

FIG. 8. (a) Thermoelectric figure-of-merit (zT) and (b) lattice thermal conductivity as a function of the configurational entropy in conventional multicomponent thermoelectric materials (adapted with permission from Ref. 73).

electronic properties. Chen et al.[11] investigated the superconductivity of various HEAs (NbTaTiZr, GeNbTaTiZr, HfNbTaTiZr, and HfGeNbTaTiVZr) in as-cast and homogenized conditions. They found that T_t is higher than predicted by the rule of mixtures (RoM). Guo et al.[77] reported that $(NbTa)_{0.67}(HfTiZr)_{0.33}$ shows extraordinarily robust zero-resistance superconductivity after pressurizing. The value of T_t increased from an initial temperature of 7.7 K at ambient pressure to 10 K at ~60 GPa, and then slowly decreased to 9 K at 190.6 GPa. They concluded that the continuous change in zero-resistance superconductivity is due to a combination of the electronic and mechanical characteristics of HEAs. They subsequently pointed out that this unique behavior may pose a challenge to existing superconductor theories. Vrtnik et al.[78] investigated superconductivity in Ta–Nb–Hf–Zr–Ti HEA system. All samples exhibited superconductivity despite different crystal structures, indicating that the superconductivity of the Ta–Nb–Hf–Zr–Ti HEA system is insensitive to the structure. They found that minimizing the mixing enthalpy and maximizing the mixing entropy were both critical.

The Cava research group[79–81] has investigated the compositional dependence of superconducting behavior in A2 $(NbTa)_{1-x}(HfTiZr)_x$,[79] A2 $Al_x(NbTa)_{0.67}(HfTiZr)_{0.33}$,[80] B2 $(NbScZr)_{1-x}(PdRh)_x$,[81] and B2 $(NbScTaZr)_{1-x}(PdRh)_x$.[81] Their critical transition temperatures versus valence electron counts are summarized in Fig. 9 in comparison with the trend lines for binary crystalline alloys[82] and amorphous films.[83] For A2 HEAs, T_t increases with increasing valence electron counts, agreeing with the trends reported in binary crystalline alloys and amorphous alloys. However, for B2-structured HEAs, T_t increases with decreasing valence electron counts, which is counterintuitive.

For complex HEAs, the preparation and verification of SMs is a huge workload. Each additional element contributes an additional degree of freedom, lengthening the exploratory process. A more effective approach is needed for screening potential high-entropy SMs. In the field of semiconductors, Xiang et al.[84] achieved the combinatorial synthesis of semiconductor materials through combining thin film growth and physical masking techniques. It is possible that this approach can be adapted to the preparation of HEA superconductors. Through film growth techniques, a superconducting coating with a continuous compositional gradient could be deposited on the tape substrate. The mode of "single-preparation, multiple-samples" may accelerate the development of superconducting high-entropy materials.

The study of HEAs as SMs is still at a very early research stage compared to studies of HEAs for other functional applications. It may be appropriate to work within the starting points suggested at the beginning of this section, and apply thermodynamic and perhaps Fermi surface modeling, to identify potential high-entropy superconductors, coupled with high-throughput experimental methods. The apparent stability of HEAs suggests an interesting avenue for theoretical investigation. The mechanism of superconductivity of HEAs under high pressure or other extreme conditions is not yet understood, which indicates the need for further investigation.

VI. HYDROGEN STORAGE

Hydrogen storage materials are materials capable of absorbing and storing large quantities of hydrogen with minimal damage, and releasing the hydrogen as needed. They undergo hydrogenation at modest temperatures and pressures. When the alloys absorb hydrogen, their lattices expand, causing swelling and possible pulverization of the crystal structure. The desired properties for hydrogen storage alloys then are as follows: (i) a high storage capacity accessible at modest temperatures and pressures; (ii) reversibility, or the ability to release the hydrogen (again without extreme inputs); and (iii) a structural resiliency that minimizes pulverization.

To date, the reports on the hydrogen storage properties of HEAs are limited, including: BCC structures such as

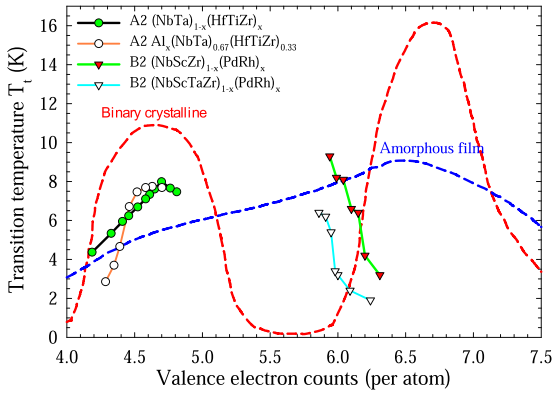

FIG. 9. Superconducting critical transition temperature (T_t) versus valence electron counts per atom of reported HEAs [$(NbTa)_{1-x}(HfTiZr)_x$,[79] $(NbScZr)_{1-x}(PdRh)_x$,[81] and $(NbScTaZr)_{1-x}(PdRh)_x$[81]] and $Al_x(NbTa)_{0.67}(HfTiZr)_{0.33}$[80] in comparison with binary crystalline alloys[82] and amorphous films[83] (adapted with permission from Ref. 81).

HfNbTiVZr[85] and MoNbTiVZr,[86] and C14 Laves structures such as CrFeNiTiVZr,[87] $CoFeMnTi_xVZr$ ($0.5 \le x \le 2.5$),[88] $CoFeMnTiV_yZr$ ($0.4 \le y \le 3.0$),[88] and $CoFeMnTiVZr_z$ ($0.4 \le z \le 3.0$).[88] Other examples include the La–Fe–Mn–Ni–V HEAs[89] which have σ + $La(Ni,Mn)_5$ or FCC + $La(Ni,Mn)_5$ phases in the microstructure.

Among these alloys studied, HfNbTiVZr shows an outstanding hydrogen absorption (~2.7 wt%), greater than any of its constituent elements will singly absorb.[85] It was hypothesized that the large lattice distortion (i.e., the difference in atomic radii of the elements δ = 6.82%) in the alloy makes it favorable to absorb hydrogen in both tetrahedral and octahedral interstitial sites. Contrasted to HfNbTiVZr is the low hydrogen capacity of MoNbTiVZr, whose maximum hydrogen absorption is merely 0.59–0.61 wt%.[86] The C14-based HEAs have a maximum hydrogen capacities ranging from 1.56 to 1.80 wt%.[88]

Refractory BCC metals have extremely large hydrogen solubility according to the established binary phase diagrams.[90] For example, pure V shows gravimetric storage capacity of >4 wt%, greater than AB_2 and AB_5 compounds.[91] Thus V-based solid solution alloys have been extensively studied for hydrogen storage to enhance the reversibility as compared to pure V, and to prevent pulverization. Addition of many alloying elements Ti, Mn, Zr, Cr, Co, Ni, Fe, Mo, Nb, Al, and Si have been studied, and these alloys are basically low- and medium-entropy alloys.[91] The two alloys studied by Luo et al.[92] [i.e., $(FeV)_{0.6}(CoCrTi)_{0.4}$ and $(FeV)_{0.6}(CoCrTi)_{0.38}Zr_{0.02}$] are actually HEAs since they have configurational entropy ~$1.6k_B$ even though "HEA" was not mentioned in the paper.

The comparison in the reported reversible hydrogen storage capacity for a variety of V-based solid solution alloys, the maximum hydrogen absorption of HEAs, and selected Ti-based BCC solid solution[93] at 298 K are shown in Fig. 10. HfNbTiVZr has significantly larger hydrogen capacity than MoNbTiVZr. This is understandable since BCC Mo and Nb metals have extremely small hydrogen solubility, while BCC Hf, Ti, Zr, and V metals have extremely large hydrogen solubility. However, the maximum hydrogen capacity of the La–Fe–Mn–Ni–V HEAs based on $LaNi_5$[89] are apparently lower than $LaNi_5$, partly due to the formation of σ and FCC phases whose hydrogen solubility is low.

At T = 298 K, most V-rich solid solution alloys exhibit significantly improved reversible capacity compared to pure V at 313 K, demonstrating that increasing the configurational entropy of the solid solution phase favors hydrogen absorption. However, exceptions to this occur for $(V_{0.645}Ti_{0.355})_{93}Co_7$ and $(V_{0.645}Ti_{0.355})_{93}Ni_7$ at 298 K[91] (see Fig. 10) and $V_{0.40}Ti_{0.225}Cr_{0.325}Fe_{0.05}$ at 303 K[91] (not shown). By contrast, for the five Ti-based BCC solid solution alloys, hydrogen capacity decreases with increasing entropy.

These results indicate that entropy could contribute to hydrogen absorption favorably, but there are other factors that are also important such as the enthalpies of formation for the solid solution (with dissolved hydrogen) and metal hydrides. In fact, enthalpies impact significantly on the hydrogen solubility as summarized by Kao et al.[88] who showed the maximum hydrogen storage (per atom) increases with decreasing the enthalpy of formation (toward more negative) for the conventional compounds and HEAs they studied. Kumar[91] concluded that an optimal performance in balanced reversible hydrogen capacity, dehydrogenation plateau pressure, pulverization resistance, and adsorption kinetics can be achieved by a material containing both alloying elements that have higher affinity for hydrogen (e.g., Ti, Zr, and Nb) and those that have less affinity (e.g., Mn, Al, and Cr).

Although FCC HEAs are not intended for hydrogen storage purposes, recent work indicates that FCC HEAs can be strong, ductile, and hydrogen tolerant materials.[94–96] Hydrogen is detrimental to metals and alloys during service due to hydrogen-induced embrittlement. Hydrogen is ubiquitous and enters into metals, forming voids, enabling void coalescence, as well as combining with certain elements to form metal hydrides. FCC HEAs such as CoCrFeMnNi are reported to be immune to hydrogen embrittlement.[94–96] Luo et al.[94] reported that hydrogen improves the strength and ductility of the alloy by simultaneously decreasing the phase stability of the FCC structure and triggering more intense nano-twinning upon loading. Zhao et al.[96] reported that the FCC CoCrFeMnNi HEA demonstrated superior resistance to gaseous hydrogen embrittlement relative to two austenitic stainless steels due to a hydrogen-enhanced localized plasticity deformation mechanism, despite the HEAs absorbing more hydrogen than the two steels.

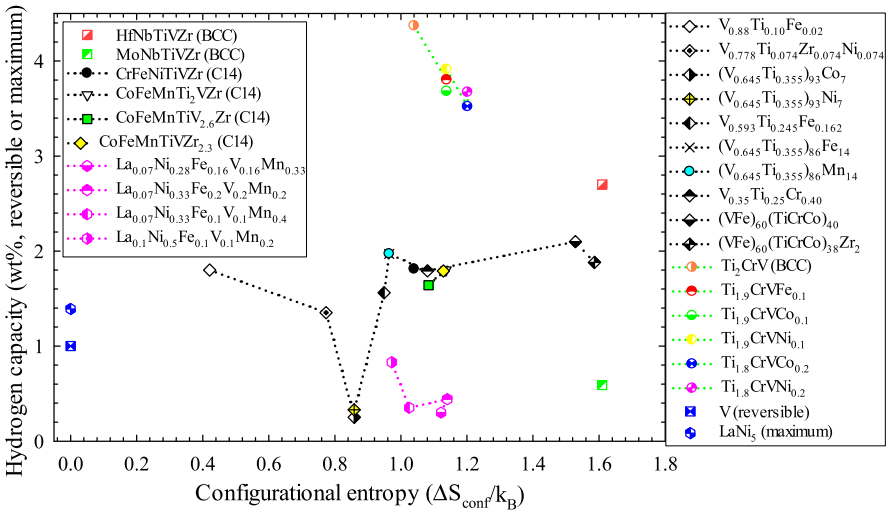

FIG. 10. Maximum hydrogen storage capacity of reported HEAs at $T = 298$ K versus reversible hydrogen storage capacity for a variety of V-based solid solution alloys[91] at $T = 298$ K and the maximum hydrogen storage capacity of BCC Ti-based alloys[93] in relation to the configurational entropy of the alloys (data taken from Refs. 91 and 93).

VII. OTHER FUNCTIONAL MATERIALS

A. Connection to conventional functional materials

Earlier sections in this review discussed functional alloys that are motivated and informed by the HEA strategy of devising alloys with multiple principal elements. However, functional HEAs have also been produced by the conventional functional materials community using concepts that are completely independent of high-entropy concepts (examples shown in earlier sections[61,71–73,92]). In fact, some of these functional HEAs have been produced before the HEA field was initiated in 2004. The purpose of this section is to further illustrate these additional 'hidden' functional HEAs, which may be missed by conventional literature searches, and to discuss the guiding principles that have been used to produce them.

Most functional materials have a long-range ordered crystal structure. Presented herein are just a few examples of functional properties, the ordered crystal structures associated with them, and typical base compounds. These examples include shape memory alloys (cesium chloride and NiTi), ferroelectric materials (perovskite and $PbTiO_3$), transparent conducting oxides (bixbyite and In_2O_3), thermoelectric materials (skudderudite, $CoAs_3$ or half-Heusler, and NbCoSn), ferromagnetic shape memory compounds (Heusler, Ni_2MnGa, and Co_2MnGe), and integrated circuit dielectric materials (beta cristobalite and SiO_2).

Over the past several decades, well-established alloying approaches have been established to improve the balance of functional properties in ordered compounds. Two general alloying approaches include doping[97] and iso-electronic (also called iso-structure) substitution.[98] Simply stated, the iso-electronic concept mixes two or more chemically or electronically similar elements on a specific sublattice of an ordered crystal structure. In both doping and iso-electronic approaches, alloying elements are selected based on considerations that include their influence on the electronic structure of the compound or the charge carrier density, atomic size, and the ability to retain the crystal structure of the host compound. Important features in both approaches include the concentrations of elemental substitutions, the sublattice in the ordered structure targeted by the alloying additions, and the number of candidate alloying elements that satisfy the alloying strategy.

Some functional material compounds have only two sublattices and some have as many as four sublattices. Some compounds have only 1 or 2 elements that have been substituted on one of the sublattices, while other compounds have a number of different elements that can be substituted on each of the distinct sublattices. Finally, doping and iso-electronic alloying approaches can range from minor solute additions to concentrated alloys. Taken together, these considerations show that traditional alloying approaches for functional materials can produce compositions that satisfy HEA definitions. For example, iso-electronic alloying has produced thermoelectric materials such as $Co(Hf_{0.5}Zr_{0.5})(Sb_{0.8}Sn_{0.2})$, $(Co_{0.95}Ni_{0.05})(Hf_{0.25}Ti_{0.5}Zr_{0.25})Sb$, and $(Co_{0.87}Ni_{0.13})(Hf_{0.4}Ti_{0.6})Sb$[99] all of which meet standard HEA definitions. These alloys represent the much larger family of half-Heusler phases that can be listed as *XYZ*, where *X* sublattice sites are occupied by Au, Co, Fe, Ir, Ni, Pd, Pt, Rh, and/or Ru; *Y* sites contain Hf, Mn, Ti, and/or Zr; and *Z* sites can be filled by Bi, Ga, Sb, and/or Sn.[100] In the same way,

skudderudite compounds can be listed as (Co,Fe,Ni)(As,P,Sb)$_3$ and Heusler phases can be represented as (Co,Cu,Fe,Ni,Pd)$_2$(Fe,Mn,V)(Al,Ga,Ge,In,Sb,Si,Sn). It is clear that a large number of functional HEAs can be produced from compounds such as these.

B. High-entropy ceramics

Oxide compounds possess a wide range of functional properties that include piezoelectric, dielectric, ferroelectric, ferromagnetic, luminescent, or phosphorescent behaviors and are a very important group of functional materials. By engineering atomic mixing on the cation sublattice of oxide compounds, the field of high-entropy oxides has recently been launched.[101–107] High-entropy concepts are now being used to design new oxide materials with functional properties,[102] high-entropy metal diborides,[108] high-entropy carbides and nitrides,[20,109–116] and other high-entropy compounds,[117,118] further expanding the impact of high-entropy concepts into the functional materials realm.

The concept of entropy stabilization is a major, new contribution from the HEA field and is clearly demonstrated in a single-phase rock-salt structure (CoCuMgNiZn)O, where the five constituent binary oxides include three different crystal structures: tenorite (CuO); wurtzite (ZnO); and rock-salt (CoO, MgO, NiO).[101] The configurational entropy from mixing on the cation sublattice in (CoCuMgNiZn)O is able to dissolve CuO and ZnO into the rock-salt structure. Entropy stabilization has also been shown in multicomponent, equiatomic rare earth oxides, where single-phase, CaF_2-type structures are produced in as-synthesized (CeLaPr)O, (CeLaPrY)O, (CeLaPrSm)O, (CeLaSmY)O, (CeLaPrSmY)O, (CeLaNdPrSmY)O, and (CeGdLaNdPrSmY)O.[104] Annealing experiments in the latter three compositions suggest that additional factors beyond configurational entropy play important roles in phase equilibria, including oxidation states of the constituent elements, synthesis procedure, and crystallite size.

VIII. SUMMARIES AND PERSPECTIVES

In summary, soft magnetic properties, MCE, thermoelectric properties, superconducting behavior, and hydrogen storage of HEAs were discussed herein. Connection to, and comparison with, traditional functional materials were provided where available. Increasing entropy is seen to impact favorably and sometimes unfavorably, the functional properties in both high-entropy and conventional functional materials.

However, entropy does not always dominate the functional properties. Doping, or isoelectronic (or isostructural) substitution, are commonly used for new materials exploration, which inevitably changes the entropy, and most often changes the enthalpy and electronic structure as well. Predictive computational modeling such as first-principles DFT reveals that the functional and physical properties are closely related to the electronic structures of the alloys.[63] High-throughput DFT calculations on HEA or MPEA functional materials can be used to predict electronic structures, and hence, the functional properties. While computationally intense, this approach can be used to accelerate discovering next-generation high-performance functional materials.

To date, single-phase high-entropy solid solution alloys are indeed very limited[3] because entropy does not always dominate phase stability.[119] One feasible approach for exploring next-generation functional materials may be to start from existing low- or medium-entropy functional materials and use rational substitution or doping. To ensure effective, and favorable, substitution to produce the desired functional property, multiscale computer modeling using DFT,[37,46,56,58,63,65,120–122] molecular dynamics,[46,123–125] hybrid Monte Carlo/molecular dynamics,[3,126,127] CALPHAD,[128,129] and phase diagram inspection[130] will serve as the starting point in a process to streamline and more efficiently screen potential candidate alloys.

A very large number of functional compounds do not satisfy rigorous HEA definitions but are nevertheless consistent with MPEA concepts. Such functional MPEAs may have fewer than 5 principal elements or have an element with >35% concentration. These functional materials are discussed in review articles such as in Ref. 2 but are generally not identified as MPEAs or HEAs in the traditional functional materials literature. Furthermore, "high-entropy" ceramics (i.e., oxides, nitrides, carbides, and borides) typically have anion concentrations above 35% and are thus not high-entropy "alloys" by conventional definitions. Nevertheless, the ability to produce unusual, useful properties in multiprincipal element functional materials is an important result worthy of additional study. Inconsistency with standard high-entropy definitions is a minor distraction at present and further study may resolve existing discrepancies. The contribution of the HEA field to functional materials goes beyond the concept of entropy stabilization and includes the potential vastness of unexplored compositions, supporting a bolder, more intentional mixing of many principal elements in functional materials.[1]

ACKNOWLEDGMENTS

This work was performed in support of the US Department of Energy's Fossil Energy Crosscutting Technology Research Program. The research was executed through the NETL Research and Innovation Center's Advanced Alloy Development Field Work Proposal. Research performed by AECOM Staff was conducted under the RES contract DE-FE0004000. X.H.Y. and Y.Z. appreciate financial support from the National Science

Foundation of China (No. 51471025) and 111 Project (B07003). D.B.M. acknowledges support from the Air Force Research Laboratory, Materials and Manufacturing Directorate. M.C.G. thanks Zhao Fan, Sheng Guo, Xun Shi, Tingting Zuo, Shengguo Ma, Hui Xu, Karoline Stolze, and Ke Jin for sharing the original data of their publications.

REFERENCES

1. J.W. Yeh, S.K. Chen, S.J. Lin, J.Y. Gan, T.S. Chin, T.T. Shun, C.H. Tsau, and S.Y. Chang: Nanostructured high-entropy alloys with multiple principal elements: Novel alloy design concepts and outcomes. *Adv. Eng. Mater.* **6**, 299 (2004).
2. B. Cantor, I.T.H. Chang, P. Knight, and A.J.B. Vincent: Microstructural development in equiatomic multicomponent alloys. *Mater. Sci. Eng., A* **375–377**, 213 (2004).
3. M.C. Gao, C. Zhang, P. Gao, F. Zhang, L.Z. Ouyang, M. Widom, and J.A. Hawk: Thermodynamics of concentrated solid solution alloys. *Curr. Opin. Solid State Mater. Sci.* **21**, 238 (2017).
4. Y. Zhang, T.T. Zuo, Z. Tang, M.C. Gao, K.A. Dahmen, P.K. Liaw, and Z.P. Lu: Microstructures and properties of high-entropy alloys. *Prog. Mater. Sci.* **61**, 1 (2014).
5. M.C. Gao, J.W. Yeh, P.K. Liaw, and Y. Zhang: *High-Entropy Alloys: Fundamentals and Applications*, 1st ed. (Springer International Publishing, Cham, 2016).
6. D.B. Miracle and O.N. Senkov: A critical review of high entropy alloys and related concepts. *Acta Mater.* **122**, 448 (2017).
7. J.W. Yeh: Physical metallurgy. In *High Entropy Alloys: Fundamentals and Applications*, M.C. Gao, J.W. Yeh, P.K. Liaw, and Y. Zhang, eds. (Springer International Publishing, Cham, 2016); p. 51.
8. D.B. Miracle, J.D. Miller, O.N. Senkov, C. Woodward, M.D. Uchic, and J. Tiley: Exploration and development of high entropy alloys for structural applications. *Entropy* **16**, 494 (2014).
9. S. Gorsse, D.B. Miracle, and O.N. Senkov: Mapping the world of complex concentrated alloys. *Acta Mater.* **135**, 177 (2017).
10. C.C. Koch: Nanocrystalline high-entropy alloys. *J. Mater. Res.* **32**, 3435 (2017).
11. J.W. Yeh, S.K. Chen, H.C. Shih, Y. Zhang, and T.T. Zuo: Functional properties. In *High Entropy Alloys: Fundamentals and Applications*, M.C. Gao, J.W. Yeh, P.K. Liaw, and Y. Zhang, eds. (Springer International Publishing, Cham, 2016); p. 237.
12. A. Perrin, M. Sorescu, M.T. Burton, D.E. Laughlin, and M. McHenry: The role of compositional tuning of the distributed exchange on magnetocaloric properties of high-entropy alloys. *JOM* **69**, 2125 (2017).
13. Y. Yuan, Y. Wu, X. Tong, H. Zhang, H. Wang, X.J. Liu, L. Ma, H.L. Suo, and Z.P. Lu: Rare-earth high-entropy alloys with giant magnetocaloric effect. *Acta Mater.* **125**, 481 (2017).
14. S. Shafeie, S. Guo, Q. Hu, H. Fahlquist, P. Erhart, and A. Palmqvist: High-entropy alloys as high-temperature thermoelectric materials. *J. Appl. Phys.* **118**, 184905 (2015).
15. Z. Fan, H. Wang, Y. Wu, X.J. Liu, and Z.P. Lu: Thermoelectric performance of PbSnTeSe high-entropy alloys. *Mater. Res. Lett.* **5**, 187 (2017).
16. Z. Fan, H. Wang, Y. Wu, X.J. Liu, and Z.P. Lu: Thermoelectric high-entropy alloys with low lattice thermal conductivity. *RSC Adv.* **6**, 52164 (2016).
17. Y. Shi, B. Yang, and P.K. Liaw: Corrosion-resistant high-entropy alloys: A review. *Metals* **7**, 43 (2017).
18. Y. Qiu, S. Thomas, M.A. Gibson, H.L. Fraser, and N. Birbilis: Corrosion of high entropy alloys. *npj Mater. Degrad.* **1**, 15 (2017).
19. A.A. Rodriguez, J. Tylczak, M.C. Gao, P.D. Jablonski, M. Detrois, M. Ziomek-Moroz, and J.A. Hawk: Effect of molybdenum on the corrosion behavior of high-entropy alloys $CoCrFeNi_2$ and $CoCrFeNi_2Mo_{0.25}$ under sodium chloride aqueous conditions. *Adv. Mater. Sci. Eng.* **2018**, 3016304 (2017).
20. J.W. Yeh, S.J. Lin, M.H. Tsai, and S.Y. Chang: High-entropy coatings. In *High Entropy Alloys: Fundamentals and Applications*, M.C. Gao, J.W. Yeh, P.K. Liaw, and Y. Zhang, eds. (Springer International Publishing, Cham, 2016); p. 469.
21. J.W. Yeh, A.C. Yeh, and S.Y. Chang: Potential applications and prospects. In *High Entropy Alloys: Fundamentals and Applications*, M.C. Gao, J.W. Yeh, P.K. Liaw, and Y. Zhang, eds. (Springer International Publishing, Cham, 2016); p. 493.
22. X.F. Wang, Y. Zhang, Y. Qiao, and G.L. Chen: Novel microstructure and properties of multicomponent CoCrCuFeNiTi_x alloys. *Intermetallics* **15**, 357 (2007).
23. C.Z. Yao, P. Zhang, M. Liu, G.R. Li, J.Q. Ye, P. Liu, and Y.X. Tong: Electrochemical preparation and magnetic study of Bi–Fe–Co–Ni–Mn high entropy alloy. *Electrochim. Acta* **53**, 8359 (2008).
24. K.B. Zhang, Z.Y. Fu, J.Y. Zhang, J. Shi, W.M. Wang, H. Wang, Y.C. Wang, and Q.J. Zhang: Annealing on the structure and properties evolution of the CoCrFeNiCuAl high-entropy alloy. *J. Alloys Compd.* **502**, 295 (2010).
25. Y.F. Kao, S.K. Chen, T.J. Chen, P.C. Chu, J.W. Yeh, and S.J. Lin: Electrical, magnetic, and Hall properties of $Al_xCoCrFeNi$ high-entropy alloys. *J. Alloys Compd.* **509**, 1607 (2011).
26. M.S. Lucas, L. Mauger, J.A. Munoz, Y. Xiao, A.O. Sheets, S.L. Semiatin, J. Horwath, and Z. Turgut: Magnetic and vibrational properties of high-entropy alloys. *J. Appl. Phys.* **109**, 07E307 (2011).
27. L. Liu, J.B. Zhu, J.C. Li, and Q. Jiang: Microstructure and magnetic properties of $FeNiCuMnTiSn_x$ high entropy alloys. *Adv. Engin. Mater.* **14**, 919 (2012).
28. S.G. Ma and Y. Zhang: Effect of Nb addition on the microstructure and properties of AlCoCrFeNi high-entropy alloy. *Mater. Sci. Eng., A* **532**, 480 (2012).
29. Y. Zhang, T.T. Zuo, Y.Q. Cheng, and P.K. Liaw: High-entropy alloys with high saturation magnetization, electrical resistivity, and malleability. *Sci. Rep.* **3**, 1455 (2013).

30. T.T. Zuo, S.B. Ren, P.K. Liaw, and Y. Zhang: Processing effects on the magnetic and mechanical properties of $FeCoNiAl_{0.2}Si_{0.2}$ high entropy alloy. *Int. J. Miner. Metall. Mater.* **20**, 549 (2013).
31. N.H. Tariq, M. Naeem, B.A. Hasan, J.I. Akhter, and M. Siddique: Effect of W and Zr on structural, thermal and magnetic properties of AlCoCrCuFeNi high entropy alloy. *J. Alloys Compd.* **556**, 79 (2013).
32. J. Wang, Z. Zheng, J. Xu, and Y. Wang: Microstructure and magnetic properties of mechanically alloyed FeSiSAlNi(Nb) high entropy alloys. *J. Magn. Magn. Mater.* **355**, 58 (2014).
33. T.T. Zuo, R.B. Li, X.J. Ren, and Y. Zhang: Effects of Al and Si addition on the structure and properties of CoFeNi equal atomic ratio alloy. *J. Magn. Magn. Mater.* **371**, 60 (2014).
34. T.T. Zuo, X. Yang, P.K. Liaw, and Y. Zhang: Influence of Bridgman solidification on microstructures and magnetic behaviors of a non-equiatomic FeCoNiAlSi high-entropy alloy. *Intermetallics* **67**, 171 (2015).
35. W. Ji, W. Wang, H. Wang, J. Zhang, Y. Wang, F. Zhang, and Z. Fu: Alloying behavior and novel properties of CoCrFeNiMn high-entropy alloy fabricated by mechanical alloying and spark plasma sintering. *Intermetallics* **56**, 24 (2015).
36. T.L. Qi, Y.H. Li, A. Takeuchi, G.Q. Xie, H.T. Miao, and W. Zhang: Soft magnetic $Fe_{25}Co_{25}Ni_{25}(B, Si)_{25}$ high entropy bulk metallic glasses. *Intermetallics* **66**, 8 (2015).
37. S. Huang, W. Li, X.Q. Li, S. Schonecker, L. Bergqvist, E. Holmstrom, L.K. Varga, and L. Vitos: Mechanism of magnetic transition in FeCrCoNi-based high entropy alloys. *Mater. Des.* **103**, 71 (2016).
38. P.F. Yu, L.J. Zhang, H. Cheng, H. Zhang, M.Z. Ma, Y.C. Li, G. Li, P.K. Liaw, and R.P. Liu: The high-entropy alloys with high hardness and soft magnetic property prepared by mechanical alloying and high-pressure sintering. *Intermetallics* **70**, 82 (2016).
39. P-C. Lin, C-Y. Cheng, J-W. Yeh, and T-S. Chin: Soft magnetic properties of high-entropy Fe–Co–Ni–Cr–Al–Si thin films. *Entropy* **18**, 308 (2016).
40. A.J. Zaddach, C. Niu, A.A. Oni, M. Fan, J.M. LeBeau, D.L. Irving, and C.C. Koch: Structure and magnetic properties of a multi-principal element Ni–Fe–Cr–Co–Zn–Mn alloy. *Intermetallics* **68**, 107 (2016).
41. P.P. Li, A.D. Wang, and C.T. Liu: A ductile high entropy alloy with attractive magnetic properties. *J. Alloys Compd.* **694**, 55 (2017).
42. R. Wei, J. Tao, H. Sun, C. Chen, G.W. Sun, and F.S. Li: Soft magnetic $Fe_{26.7}Co_{26.7}Ni_{26.6}Si_9B_{11}$ high entropy metallic glass with good bending ductility. *Mater. Lett.* **197**, 87 (2017).
43. R. Wei, H. Sun, C. Chen, Z.H. Han, and F.S. Li: Effect of cooling rate on the phase structure and magnetic properties of $Fe_{26.7}Co_{28.5}Ni_{28.5}Si_{4.6}B_{8.7}P_3$ high entropy alloy. *J. Magn. Magn. Mater.* **435**, 184 (2017).
44. R.K. Mishra and R.R. Shahi: Phase evolution and magnetic characteristics of TiFeNiCr and TiFeNiCrM (M = Mn, Co) high entropy alloys. *J. Magn. Magn. Mater.* **442**, 218 (2017).
45. P.P. Li, A.D. Wang, and C.T. Liu: Composition dependence of structure, physical and mechanical properties of $FeCoNi(MnAl)_x$ high entropy alloys. *Intermetallics* **87**, 21 (2017).
46. T.T. Zuo, M.C. Gao, L.Z. Ouyang, X. Yang, Y.Q. Cheng, R. Feng, S.Y. Chen, P.K. Liaw, J.A. Hawk, and Y. Zhang: Tailoring magnetic behaviors of CoFeMnNiX (X = Al, Ga, and Sn) high entropy alloys by metal doping. *Acta Mater.* **130**, 10 (2017).
47. C. Shang, E. Axinte, W. Ge, Z. Zhang, and Y. Wang: High-entropy alloy coatings with excellent mechanical, corrosion resistance and magnetic properties prepared by mechanical alloying and hot pressing sintering. *Surf. Interfaces* **9**, 36 (2017).
48. Q. Zhang, H. Xu, X.H. Tan, X.L. Hou, S.W. Wu, G.S. Tan, and L.Y. Yu: The effects of phase constitution on magnetic and mechanical properties of $FeCoNi(CuAl)_x$ (x = 0–1.2) high-entropy alloys. *J. Alloys Compd.* **693**, 1061 (2017).
49. O. Schneeweiss, M. Friak, M. Dudova, D. Holec, M. Sob, D. Kriegner, V. Holy, P. Beran, E.P. George, J. Neugebauer, and A. Dlouhy: Magnetic properties of the CrMnFeCoNi high-entropy alloy. *Phys. Rev. B* **96**, 014437 (2017).
50. Z. Li, H. Xu, Y. Gu, M. Pan, L. Yu, X. Tan, and X. Hou: Correlation between the magnetic properties and phase constitution of $FeCoNi(CuAl)_{0.8}Ga_x$ ($0 \le x \le 0.08$) high-entropy alloys. *J. Alloy. Comp.* **746**, 285 (2018).
51. J.W. Yeh: Alloy design strategies and future trends in high-entropy alloys. *JOM* **65**, 1759 (2013).
52. O. Gutfleisch, M.A. Willard, E. Brück, C.H. Chen, S.G. Sankar, and J.P. Liu: Magnetic materials and devices for the 21st century: Stronger, lighter, and more energy efficient. *Adv. Mater.* **23**, 821 (2011).
53. G. Herzer: Modern soft magnets: Amorphous and nanocrystalline materials. *Acta Mater.* **61**, 718 (2013).
54. M.S. Lucas, D. Belyea, C. Bauer, N. Bryant, E. Michel, Z. Turgut, S.O. Leontsev, J. Horwath, S.L. Semiatin, M.E. McHenry, and C.W. Miller: Thermomagnetic analysis of $FeCoCr_xNi$ alloys: Magnetic entropy of high-entropy alloys. *J. Appl. Phys.* **113**, 17A923 (2013).
55. D. Ma, B. Grabowski, F. Kormann, J. Neugebauer, and D. Raabe: Ab initio thermodynamics of the CoCrFeMnNi high entropy alloy: Importance of entropy contributions beyond the configurational one. *Acta Mater.* **100**, 90 (2015).
56. S. Huang, E. Holmström, O. Eriksson, and L. Vitos: Mapping the magnetic transition temperatures for medium- and high-entropy alloys. *Intermetallics* **95**, 80 (2018).
57. F. Körmann, T. Hickel, and J. Neugebauer: Influence of magnetic excitations on the phase stability of metals and steels. *Curr. Opin. Solid State Mater. Sci.* **20**, 77 (2016).
58. F. Körmann, D. Ma, D.D. Belyea, M.S. Lucas, C.W. Miller, B. Grabowski, and M.H.F. Sluiter: "Treasure maps" for magnetic high-entropy-alloys from theory and experiment. *Appl. Phys. Lett.* **107**, 142404 (2015).
59. D.D. Belyea, M.S. Lucas, E. Michel, J. Horwath, and C.W. Miller: Tunable magnetocaloric effect in transition metal alloys. *Sci. Rep.* **5**, 15755 (2015).
60. B.G. Shen, J.R. Sun, F.X. Hu, H.W. Zhang, and Z.H. Cheng: Recent progress in exploring magnetocaloric materials. *Adv. Mater.* **21**, 4545 (2009).
61. J. Shen, Y.X. Li, J.R. Sun, and B.G. Shen: Effect of R substitution on magnetic properties and magnetocaloric effects of $La_{1-x}R_xFe_{11.5}Si_{1.5}$ compounds with R = Ce, Pr, and Nd. *Chin. Phys. B* **18**, 2058 (2009).
62. K. Jin and H. Bei: Single-phase concentrated solid-solution alloys: Bridging intrinsic transport properties and irradiation resistance. *Front. Mater.* **5**, 1 (2018).
63. K. Jin, B.C. Sales, G.M. Stocks, G.D. Samolyuk, M. Daene, W.J. Weber, Y. Zhang, and H. Bei: Tailoring the physical properties of Ni-based single-phase equiatomic alloys by modifying the chemical complexity. *Sci. Rep.* **6**, 20159 (2016).
64. G.J. Snyder and E.S. Toberer: Complex thermoelectric materials. *Nat. Mater.* **7**, 105 (2008).
65. Y.W. Zhang, G.M. Stocks, K. Jin, C.Y. Lu, H.B. Bei, B.C. Sales, L.M. Wang, L.K. Beland, R.E. Stoller, G.D. Samolyuk, M. Caro, A. Caro, and W.J. Weber: Influence of chemical disorder on energy dissipation and defect evolution in concentrated solid solution alloys. *Nat. Commun.* **6**, 8736 (2015).
66. H.P. Chou, Y.S. Chang, S.K. Chen, and J.W. Yeh: Microstructure, thermophysical and electrical properties in $Al_xCoCrFeNi$

($0 \leq x \leq 2$) high-entropy alloys. *Mater. Sci. Eng., B* **163**, 184 (2009).
67. Y.Z. Pei, X.Y. Shi, A. LaLonde, H. Wang, L.D. Chen, and G.J. Snyder: Convergence of electronic bands for high performance bulk thermoelectrics. *Nature* **473**, 66 (2011).
68. D.G. Cahill, P.V. Braun, G. Chen, D.R. Clarke, S. Fan, K.E. Goodson, P. Keblinski, W.P. King, G.D. Mahan, A. Majumdar, H.J. Maris, S.R. Phillpot, E. Pop, and L. Shi: Nanoscale thermal transport. II. 2003–2012. *Appl. Phys. Rev.* **1**, 011305 (2014).
69. Z-G. Chen, G. Han, L. Yang, L. Cheng, and J. Zou: Nanostructured thermoelectric materials: Current research and future challenge. *Prog. Nat. Sci.: Mater. Int.* **22**, 535 (2012).
70. Y.Z. Pei, H. Wang, and G.J. Snyder: Band engineering of thermoelectric materials. *Adv. Mater.* **24**, 6125 (2012).
71. G.J. Tan, F.Y. Shi, S.Q. Hao, H. Chi, T.P. Bailey, L.D. Zhao, C. Uher, C. Wolverton, V.P. Dravid, and M.G. Kanatzidis: Valence band modification and high thermoelectric performance in SnTe heavily alloyed with MnTe. *J. Am. Chem. Soc.* **137**, 11507 (2015).
72. R. Orabi, J. Hwang, C.C. Lin, R. Gautier, B. Fontaine, W. Kim, J.S. Rhyee, D. Wee, and M. Fornari: Ultralow lattice thermal conductivity and enhanced thermoelectric performance in SnTe: Ga materials. *Chem. Mater.* **29**, 612 (2017).
73. R.H. Liu, H.Y. Chen, K.P. Zhao, Y.T. Qin, B.B. Jiang, T.S. Zhang, G. Sha, X. Shi, C. Uher, W.Q. Zhang, and L.D. Chen: Entropy as a gene-like performance indicator promoting thermoelectric materials. *Adv. Mater.* **29**, 1702712 (2017).
74. R. Hott, R. Kleiner, T. Wolf, and G. Zwicknagl: Superconducting materials—A topical overview. In *Frontiers in Superconducting Materials*, A.V. Narlikar, ed. (Springer, Berlin, Heidelberg, 2005); p. 1.
75. C.W. Chu, P.C. Canfield, R.C. Dynes, Z. Fisk, B. Batlogg, G. Deutscher, T.H. Geballe, Z.X. Zhao, R.L. Greene, H. Hosono, and M.B. Maple: Epilogue: Superconducting materials past, present and future. *Phys. C* **514**, 437 (2015).
76. P. Kozelj, S. Vrtnik, A. Jelen, S. Jazbec, Z. Jaglicic, S. Maiti, M. Feuerbacher, W. Steurer, and J. Dolinsek: Discovery of a superconducting high-entropy alloy. *Phys. Rev. Lett.* **113**, 107001 (2014).
77. J. Guo, H.H. Wang, F. von Rohr, Z. Wang, S. Cai, Y.Z. Zhou, K. Yang, A.G. Li, S. Jiang, Q. Wu, R.J. Cava, and L.L. Sun: Robust zero resistance in a superconducting high-entropy alloy at pressures up to 190 GPa. *Proc. Natl. Acad. Sci. U. S. A.* **114**, 13144 (2017).
78. S. Vrtnik, P. Kozelj, A. Meden, S. Maiti, W. Steurer, M. Feuerbacher, and J. Dolinsek: Superconductivity in thermally annealed Ta–Nb–Hf–Zr–Ti high-entropy alloys. *J. Alloys Compd.* **695**, 3530 (2017).
79. F. von Rohr, M.J. Winiarski, J. Tao, T. Klimczuk, and R.J. Cava: Effect of electron count and chemical complexity in the Ta–Nb–Hf–Zr–Ti high-entropy alloy superconductor. *Proc. Natl. Acad. Sci. U. S. A.* **113**, E7144 (2016).
80. F.O. von Rohr and R.J. Cava: Isoelectronic substitutions and aluminium alloying in the Ta–Nb–Hf–Zr–Ti high-entropy alloy superconductor. *Phys. Rev. Mater.* **2**, 034801 (2018).
81. K. Stolze, J. Tao, F.O. von Rohr, T. Kong, and R.J. Cava: Sc–Zr–Nb–Rh–Pd and Sc–Zr–Nb–Ta–Rh–Pd high-entropy alloy superconductors on a CsCl-type lattice. *Chem. Mater.* **30**, 906 (2018).
82. B.T. Matthias: Empirical relation between superconductivity and the number of valence electrons per atom. *Phys. Rev.* **97**, 74 (1955).
83. M.M. Collver and R.H. Hammond: Superconductivity in amorphous transition-metal alloy films. *Phys. Rev. Lett.* **30**, 92 (1973).
84. X.D. Xiang, X.D. Sun, G. Briceno, Y.L. Lou, K.A. Wang, H.Y. Chang, W.G. Wallacefreedman, S.W. Chen, and P.G. Schultz: A combinatorial approach to materials discovery. *Science* **268**, 1738 (1995).
85. M. Sahlberg, D. Karlsson, C. Zlotea, and U. Jansson: Superior hydrogen storage in high entropy alloys. *Sci. Rep.* **6**, 36770 (2016).
86. I. Kunce, M. Polanski, and J. Bystrzycki: Microstructure and hydrogen storage properties of a TiZrNbMoV high entropy alloy synthesized using Laser Engineered Net Shaping (LENS). *Int. J. Hydrogen Energy* **39**, 9904 (2014).
87. I. Kunce, M. Polanski, and J. Bystrzycki: Structure and hydrogen storage properties of a high entropy ZrTiVCrFeNi alloy synthesized using Laser Engineered Net Shaping (LENS). *Int. J. Hydrogen Energy* **38**, 12180 (2013).
88. Y.F. Kao, S.K. Chen, J.H. Sheu, J.T. Lin, W.E. Lin, J.W. Yeh, S.J. Lin, T.H. Liou, and C.W. Wang: Hydrogen storage properties of multi-principal-component $CoFeMnTi_xV_yZr_z$ alloys. *Int. J. Hydrogen Energy* **35**, 9046 (2010).
89. I. Kunce, M. Polanski, and T. Czujko: Microstructures and hydrogen storage properties of La–Ni–Fe–V–Mn alloys. *Int. J. Hydrogen Energy* **42**, 27154 (2017).
90. H. Okamoto: *Desk Handbook: Phase Diagrams for Binary Alloys* (ASM International, Materials Park, 2000).
91. S. Kumar, A. Jain, T. Ichikawa, Y. Kojima, and G.K. Dey: Development of vanadium based hydrogen storage material: A review. *Renewable Sustainable Energy Rev.* **72**, 791 (2017).
92. S. Yang, F. Yang, C. Wu, Y. Chen, Y. Mao, and L. Luo: Hydrogen storage and cyclic properties of $(VFe)_{60}(TiCrCo)_{40-x}Zr_x$ ($0 \leq x \leq 2$) alloys. *J. Alloys Compd.* **663**, 460 (2016).
93. A. Kumar, S. Banerjee, C.G.S. Pillai, and S.R. Bharadwaj: Hydrogen storage properties of $Ti_{2-x}CrVM_x$ (M = Fe, Co, Ni) alloys. *Int. J. Hydrogen Energy* **38**, 13335 (2013).
94. H. Luo, Z.M. Li, and D. Raabe: Hydrogen enhances strength and ductility of an equiatomic high-entropy alloy. *Sci. Rep.* **7**, 9892 (2017).
95. Y. Zhao, D-H. Lee, J-A. Lee, W-J. Kim, H.N. Han, U. Ramamurty, J-Y. Suh, and J-i. Jang: Hydrogen-induced nanohardness variations in a CoCrFeMnNi high-entropy alloy. *Int. J. Hydrogen Energy* **42**, 12015 (2017).
96. Y. Zhao, D.H. Lee, M.Y. Seok, J.A. Lee, M.P. Phaniraj, J.Y. Suh, H.Y. Ha, J.Y. Kim, U. Ramamurty, and J.I. Jang: Resistance of CoCrFeMnNi high-entropy alloy to gaseous hydrogen embrittlement. *Scripta Mater.* **135**, 54 (2017).
97. M.L. Green, I. Takeuchi, and J.R. Hattrick-Simpers: Applications of high throughput (combinatorial) methodologies to electronic, magnetic, optical, and energy-related materials. *J. Appl. Phys.* **113**, 231101 (2013).
98. C. Yu, T-J. Zhu, R-Z. Shi, Y. Zhang, X-B. Zhao, and J. He: High-performance half-Heusler thermoelectric materials $Hf_{1-x}Zr_xNiSn_{1-y}Sb_y$ prepared by levitation melting and spark plasma sintering. *Acta Mater.* **57**, 2757 (2009).
99. W. Xie, A. Weidenkaff, X. Tang, Q. Zhang, J. Poon, and T. Tritt: Recent advances in nanostructured thermoelectric half-heusler compounds. *Nanomaterials* **2**, 379 (2012).
100. M. Yin and P. Nash: Standard enthalpies of formation of selected XYZ half-Heusler compounds. *J. Chem. Thermodyn.* **91**, 1 (2015).
101. C.M. Rost, E. Sachet, T. Borman, A. Moballegh, E.C. Dickey, D. Hou, J.L. Jones, S. Curtarolo, and J-P. Maria: Entropy-stabilized oxides. *Nat. Commun.* **6**, 8485 (2015).
102. S.C. Jiang, T. Hu, J. Gild, N.X. Zhou, J.Y. Nie, M.D. Qin, T. Harrington, K. Vecchio, and J. Luo: A new class of high-entropy perovskite oxides. *Scripta Mater.* **142**, 116 (2018).

103. A. Sarkar, R. Djenadic, N.J. Usharani, K.P. Sanghvi, V.S.K. Chakravadhanula, A.S. Gandhi, H. Hahn, and S.S. Bhattacharya: Nanocrystalline multicomponent entropy stabilised transition metal oxides. *J. Eur. Ceram. Soc.* **37**, 747 (2017).
104. R. Djenadic, A. Sarkar, O. Clemens, C. Loho, M. Botros, V.S.K. Chakravadhanula, C. Kubel, S.S. Bhattacharya, A.S. Gandhif, and H. Hahn: Multicomponent equiatomic rare earth oxides. *Mater. Res. Lett.* **5**, 102 (2017).
105. D. Berardan, A.K. Meena, S. Franger, C. Herrero, and N. Dragoe: Controlled Jahn–Teller distortion in (MgCoNiCuZn)O-based high entropy oxides. *J. Alloys Compd.* **704**, 693 (2017).
106. D. Berardan, S. Franger, D. Dragoe, A.K. Meena, and N. Dragoe: Colossal dielectric constant in high entropy oxides. *Phys. Status Solidi Rapid Res. Lett.* **10**, 328 (2016).
107. G. Anand, A.P. Wynn, C.M. Handley, and C.L. Freeman: Phase stability and distortion in high-entropy oxides. *Acta Mater.* **146**, 119 (2018).
108. J. Gild, Y. Zhang, T. Harrington, S. Jiang, T. Hu, M.C. Quinn, W.M. Mellor, N. Zhou, K. Vecchio, and J. Luo: High-entropy metal diborides: A new class of high-entropy materials and a new type of ultrahigh temperature ceramics. *Sci. Rep.* **6**, 37946 (2016).
109. K.H. Cheng, C.H. Lai, S.J. Lin, and J.W. Yeh: Recent progress in multi-element alloy and nitride coatings sputtered from high-entropy alloy targets. *Ann. Chimie Sci. Matériaux* **31**, 723 (2006).
110. C.H. Lai, S.J. Lin, J.W. Yeh, and A. Davison: Effect of substrate bias on the structure and properties of multi-element (AlCrTaTiZr)N coatings. *J. Phys. D: Appl. Phys.* **39**, 4628 (2006).
111. C.H. Lai, K.H. Cheng, S.J. Lin, and J.W. Yeh: Mechanical and tribological properties of multi-element (AlCrTaTiZr)N coatings. *Surf. Coating. Technol.* **202**, 3732 (2008).
112. M.H. Tsai, C.H. Lai, J.W. Yeh, and J.Y. Gan: Effects of nitrogen flow ratio on the structure and properties of reactively sputtered $(AlMoNbSiTaTiVZr)N_x$ coatings. *J. Phys. D: Appl. Phys.* **41**, 235402 (2008).
113. M.H. Tsai, C.W. Wang, C.H. Lai, J.W. Yeh, and J.Y. Gan: Thermally stable amorphous $(AlMoNbSiTaTiVZr)_{50}N_{50}$ nitride film as diffusion barrier in copper metallization. *Appl. Phys. Lett.* **92**, 052109 (2008).
114. P.K. Huang and J.W. Yeh: Effects of substrate temperature and post-annealing on microstructure and properties of (AlCrNbSiTiV)N coatings. *Thin Solid Films* **518**, 180 (2009).
115. P.K. Huang and J.W. Yeh: Effects of nitrogen content on structure and mechanical properties of multi-element (AlCrNbSiTiV)N coating. *Surf. Coating. Technol.* **203**, 1891 (2009).
116. P.K. Huang and J.W. Yeh: Inhibition of grain coarsening up to 1000 °C in (AlCrNbSiTiV)N superhard coatings. *Scripta Mater.* **62**, 105 (2010).
117. A. Takeuchi, K. Amiya, T. Wada, and K. Yubuta: Alloy design for high-entropy alloys based on Pettifor map for binary compounds with 1:1 stoichiometry. *Intermetallics* **66**, 56 (2015).
118. A. Takeuchi, T. Wada, and Y. Zhang: MnFeNiCuPt and MnFeNiCuCo high-entropy alloys designed based on $L1_0$ structure in Pettifor map for binary compounds. *Intermetallics* **82**, 107 (2017).
119. F. Otto, Y. Yang, H. Bei, and E.P. George: Relative effects of enthalpy and entropy on the phase stability of equiatomic high-entropy alloys. *Acta Mater.* **61**, 2628 (2013).
120. R. Feng, P.K. Liaw, M.C. Gao, and M. Widom: First-principles prediction of high-entropy-alloy stability. *npj Comput. Mater.* **3**, 50 (2017).
121. M.C. Gao, P. Gao, J.A. Hawk, L.Z. Ouyang, D.E. Alman, and M. Widom: Computational modeling of high-entropy alloys: Structures, thermodynamics and elasticity. *J. Mater. Res.* **32**, 3627 (2017).
122. F.Y. Tian, Y. Wang, D.L. Irving, and L. Vitos: Applications of coherent potential approximation to HEAs. In *High-Entropy Alloys: Fundamentals and Applications*, M.C. Gao, J.W. Yeh, P.K. Liaw, and Y. Zhang, eds. (Springer International Publishing, Cham, 2016); p. 299.
123. M.C. Gao, B. Zhang, S.M. Guo, J.W. Qiao, and J.A. Hawk: High-entropy alloys in hexagonal close packed structure. *Metall. Mater. Trans. A* **47**, 3322 (2016).
124. L.J. Santodonato, Y. Zhang, M. Feygenson, C.M. Parish, M.C. Gao, R.J.K. Weber, J.C. Neuefeind, Z. Tang, and P.K. Liaw: Deviation from high-entropy configurations in the atomic distributions of a multi-principal-element alloy. *Nat. Commun.* **6**, 5964 (2015).
125. W.M. Choi, Y.H. Jo, S.S. Sohn, S. Lee, and B.J. Lee: Understanding the physical metallurgy of the CoCrFeMnNi high-entropy alloy: An atomistic simulation study. *npj Comput. Mater.* **4**, 1 (2018).
126. M. Widom, W.P. Huhn, S. Maiti, and W. Steurer: Hybrid Monte Carlo/molecular dynamics simulation of a refractory metal high entropy alloy. *Metall. Mater. Trans. A* **45**, 196 (2014).
127. W.P. Huhn and M. Widom: Prediction of A2 to B2 phase transition in the high-entropy alloy Mo–Nb–Ta–W. *JOM* **65**, 1772 (2013).
128. O.N. Senkov, J.D. Miller, D.B. Miracle, and C. Woodward: Accelerated exploration of multi-principal element alloys with solid solution phases. *Nat. Commun.* **6**, 6529 (2015).
129. C. Zhang and M.C. Gao: CALPHAD modeling of high-entropy alloys. In *High-Entropy Alloys: Fundamentals and Applications*, M.C. Gao, J.W. Yeh, P.K. Liaw, and Y. Zhang, eds. (Springer International Publishing, Cham, 2016); p. 399.
130. M.C. Gao and D.E. Alman: Searching for next single-phase high-entropy alloy compositions. *Entropy* **15**, 4504 (2013).